INVESTIGATION OF MARANGONI-INDUCED FLOWS IN VERTICAL MICROCHANNELS

A THESIS SUBMITTED TO
THE GRADUATE SCHOOL OF NATURAL AND APPLIED SCIENCES
OF
MIDDLE EAST TECHNICAL UNIVERSITY

BY

AYŞE UĞUR

IN PARTIAL FULFILLMENT OF THE REQUIREMENTS
FOR
THE DEGREE OF MASTER OF SCIENCE
IN
MECHANICAL ENGINEERING

AUGUST 2022

Approval of the thesis:

INVESTIGATION OF MARANGONI-INDUCED FLOWS IN VERTICAL MICROCHANNELS

submitted by **AYŞE UĞUR** in partial fulfillment of the requirements for the degree of **Master of Science in Mechanical Engineering Department, Middle East Technical University** by,

Prof. Dr. Halil Kalıpçılar
Dean, Graduate School of **Natural and Applied Sciences** _____

Prof. Dr. M. A. Sahir Arıkan
Head of Department, **Mechanical Engineering** _____

Assoc. Prof. Dr. Özgür Bayer
Supervisor, **Mechanical Engineering, METU** _____

Prof. Dr. Selin Aradağ Çelebioğlu
Co-supervisor, **Mechanical Engineering, TED University** _____

Examining Committee Members:

Prof. Dr. İlker Tarı
Mechanical Engineering, METU _____

Assoc. Prof. Dr. Özgür Bayer
Mechanical Engineering, METU _____

Prof. Dr. Selin Aradağ Çelebioğlu
Mechanical Engineering, TED University _____

Assist. Prof. Dr. Özgür Uğraş Baran
Mechanical Engineering, METU _____

Assist. Prof. Dr. Ali Karakuş
Mechanical Engineering, METU _____

17.08.2022

I hereby declare that all information in this document has been obtained and presented in accordance with academic rules and ethical conduct. I also declare that, as required by these rules and conduct, I have fully cited and referenced all material and results that are not original to this work.

Name, Surname: Ayşe Uğur

Signature :

ABSTRACT

INVESTIGATION OF MARANGONI-INDUCED FLOWS IN VERTICAL MICROCHANNELS

Uğur, Ayşe
M.S., Department of Mechanical Engineering
Supervisor: Assoc. Prof. Dr. Özgür Bayer
Co-Supervisor: Prof. Dr. Selin Aradağ Çelebioğlu

August 2022, 73 pages

Marangoni convection is defined as the tendency of movement within a fluid from the regions of lower surface tension to those of higher locations. In literature, there are various studies related to Marangoni convection in horizontal microfluidic and microgravity systems. However, the researches about Marangoni convection in vertical flows for closed systems are relatively fewer in number. In this study, Marangoni effect due to temperature gradient is numerically investigated through a fluid-fluid interface in a vertical microchannel made of polydimethylsiloxane (PDMS). Marangoni-induced flow is created by forming an interface between air and water, due to Cassie-Baxter state observed in the hydrophobic surfaces. Firstly, a validation study is performed using experimental data in the literature for a horizontal setup. For various sizes of a vertical microchannel, Marangoni convection is numerically investigated to analyse flow characterization and its effect on temperature and velocity profiles.

Keywords: Marangoni Convection, Cassie-Baxter State, Microfluidics

ÖZ

DİKEY MİKROKANALLARDA MARANGONİ-ETKİLİ AKIŞLARIN ARAŞTIRILMASI

Uğur, Ayşe
Yüksek Lisans, Makina Mühendisliği Bölümü
Tez Yöneticisi: Doç. Dr. Özgür Bayer
Ortak Tez Yöneticisi: Prof. Dr. Selin Aradağ Çelebioğlu

Ağustos 2022 , 73 sayfa

Marangoni taşınımı, bir sıvı içindeki düşük yüzey gerilimli bölgelerden yüksek gerilimli bölgelere doğru hareket eğilimi olarak tanımlanır. Literatürde, özellikle yerçekimsiz ortamda, açık, yatay veya mikro sistemler için Marangoni taşınımı incelenmiştir. Diğer taraftan, dikey kapalı sistemdeki akışlardaki etkisini inceleyen çalışmalar nispeten azdır. Bu çalışmada, polidimetilsiloksan (PDMS) dikey bir mikrokanalda, sıvı-akışkan ara yüzeyindeki sıcaklık gradyanı aracılığıyla oluşan Marangoni etkisi sayısal olarak incelenmiştir. Marangoni etkili akış, mikrokanal içerisindeki hava ve çalışma sıvısı arasında bir arayüz oluşturarak elde edilir. Bu arayüzün oluşmasını hidrofobik yüzeylerde gözlemlenen Cassie-Baxter durumu açıklamaktadır. Mikrokanalın farklı boyutlarıyla ve farklı sıcaklık farklarıyla gerçekleştirilen simulasyonlar sonucu Marangoni etkisinin akış karakterine, sıcaklık ve hız profillerine etkisi araştırılır.

Anahtar Kelimeler: Marangoni Taşınımı, Cassie-Baxter Modeli, Mikroakışkanlar

To each hair that turns gray for academic reasons

ACKNOWLEDGMENTS

I would like to thank my supervisor, Assoc. Prof. Dr. Özgür Bayer, and co-supervisor, Prof. Dr. Selin Aradağ Çelebioğlu, for their support and patience. Also, I owe you a debt of gratitude for my lovely family, my motivation fairy, İrem Karakaya, my friend in need, Seyedmohsen Baghaei Oskouei, Mustafa Yalçın and for all members of Dr. Bayer's Research Group.

TABLE OF CONTENTS

LIST OF TABLES

TABLES

LIST OF FIGURES

FIGURES

LIST OF ABBREVIATIONS

2D	2 Dimensional
3D	3 Dimensional
PDMS	Polydimethylsiloxane
Temp.	Temperature
FEM	Finite element method

LIST OF SYMBOLS

γ	Surface tension, N/m
T	Temperature, K
Θ	Young's contact angle, $\deg$
L	Microchannel length, m
W	Water width, m
d	Water depth, m
a	Air cavity height, m
b	Air cavity width, m
c	Solid partition height, m
λ	Mean free path length, m
L_c	Characteristic length, m
A_c	Cross-sectional area, m^2
P_{wetted}	Wetted perimeter, m
$\vec{V}$	Velocity vector, m/s
ρ	Density, kg/m^3
$\vec{g}$	Gravity vector, m/s^2
μ	Dynamic viscosity, $Pa.s$
x	Distance in x-direction, m
y	Distance in y-direction, m
z	Distance in z-direction, m
P	Pressure, Pa
P_c	Critical pressure, Pa
C_p	Specific heat capacity, $J/(kg.K)$

k	Thermal conductivity, $W/(m.K)$
ΔT	Temperature difference, K
α	Thermal diffusivity, m^2/s
Ω	Dimensionless velocity in z-direction
ζ	Dimensionless z-coordinate
Φ	Dimensionless temperature
f	Fraction of wetted solid in the unit cell of the microchannel
T^*	Nondimensional temperature
z^*	Nondimensional distance

LIST OF SUBSCRIPTS

x	x-direction
y	y-direction
z	z-direction
air-water	Interface between air and water
siliconoil-water	Interface between silicone oil and water
dodecanol-water	interface between dodecanol and water
LV	Liquid-vapor
SV	Solid-vapor
SL	Solid-liquid

CHAPTER 1

INTRODUCTION

1.1 Background

1.1.1 Microfluidics

Microfluidics is the science concerning the systems that process or manipulate small volumes of fluid through channels with tens to hundreds of micrometres in diameter [1]. The diagram in Figure 1.1 depicts the size of microfluidics with respect to other common sizes.

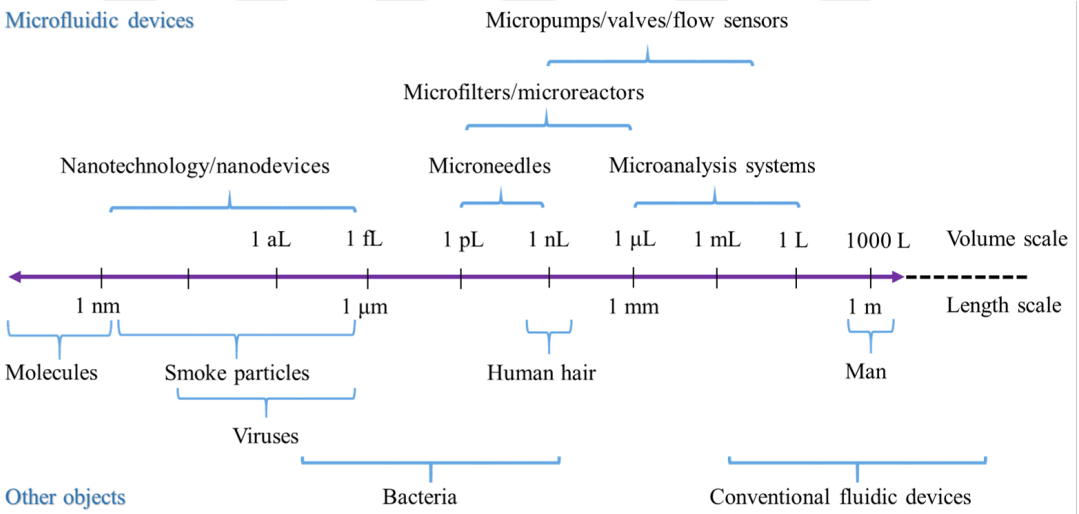

Figure 1.1: The analysis of microfluidics in terms of length and volume scales, adapted from [2]

Compared to the macroscopic systems, microfluidics scale has a number of differences. First, Reynolds number decreases as the characteristic sizes of the system is lowered. Thus, it is highly possible that laminar flow regime assumption can be

used for the analysis of the system. Accordingly, it results in solving the governing equations with minimal effort. The second difference is the dominated forces. In macroscopic systems, the gravity has a great dominancy against the surface tension and capillary forces, but in microfluidics, it is the opposite. And at last, reaction times are significantly faster in microfluidics than their conventional counterparts due to relatively shorter diffusion time resulted from the smaller dimensions of the systems [3]. The significant number of the developments in microfluidics emerged towards the end of twenties; however, its outbreak is related with the advancement in microelectronics as well integrated circuits. The manufacturing of these microsystems permits the components to be fabricated with a 1 μm precision. After the improvements in silicon fabrication and photolithography, the enhancement in production of microsystems have continued at a rapid pace [4] as depicted in Figure 1.2.

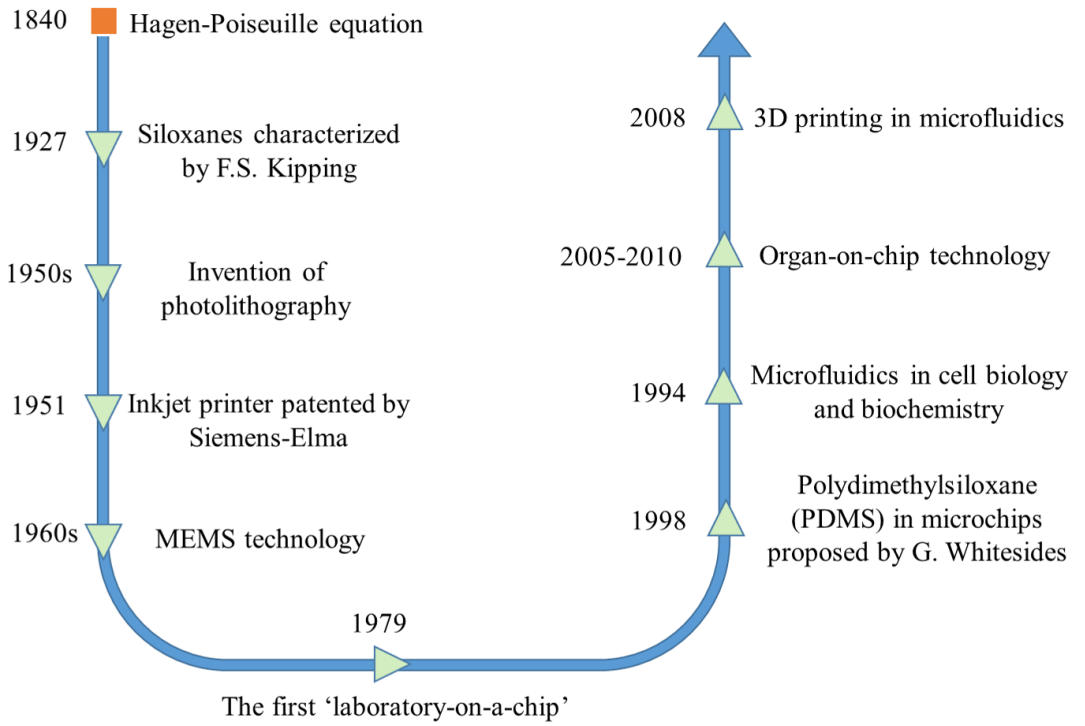

Figure 1.2: The chronologic development in microfluidics, adapted from [4]

The advances in microfluidics have heralded a multitude of exciting and novel opportunities in future. Foremost one of those is the implementation of the current technology for solving the problems in biochemistry and biomedicine. Besides, it offers a variety of brand-new potentials in different areas. One of them is the analy-

sis of the interaction between the microfluidics systems and microelectronic devices. Secondly, some specialized methods can be used for biochemical synthesis. Furthermore, it combines optical and electromagnetic technologies in chip-based gadgets in order to manipulate the samples as well analyze them [3].

1.1.2 Surface Tension

Molecules inside a fluid are kept together via the intermolecular forces balanced in all direction as in Figure 1.3. The forces on the surface of the fluid are unbalanced. This results in a tension called surface tension providing to minimize the surface of the fluid. As the term is called, surface tension is used for fluids, whereas, free surface energy is used for solids [5].

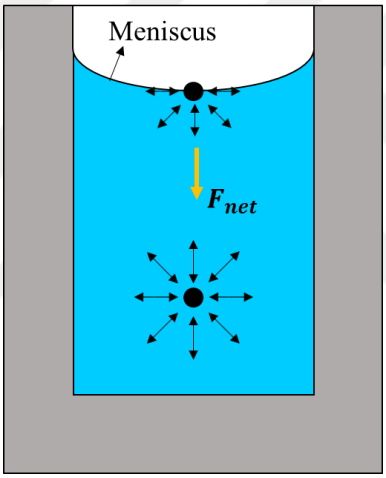

Figure 1.3: Surface tension on the surface of a fluid due to unbalanced forces, adapted from [5]

Surface tension is dependent on different conditions like temperature or concentration gradient in the system. In the current work, the temperature effect on surface tension will be focused on. Mostly, surface tension between two fluids decreases as the temperature increases such as surface tension of air-water [6]. However some fluids called self-rewetting have an opposite relation, namely surface tensions of silicon oil-water [7] and dodecanol-water [8]. For those fluids, surface tension rises in the case of temperature increase. In order to understand how the surface tension alters for the fluids having different characteristics, some experiments were conducted. As a re-

sult of the experiments, Eqn. 1.1 [6], Eqn. 1.2 [7] and Eqn. 1.3 [8] were obtained as a function of temperature, in Kelvins, for surface tension of air-water, silicon oil-water and dodecanol-water, respectively.

$$\sigma_{air-water} = 235.8(\frac{647.15 - T}{647.15})^{1.256}(1 - 0.625\frac{647.15 - T}{647.15}) \tag{1.1}$$

$$\sigma_{siliconoil-water} = 0.122T + 32.82 \tag{1.2}$$

$$\sigma_{dodecanol-water} = -8.70410^{-4}T^2 + 15.5810^{-2}T + 4.3 \tag{1.3}$$

1.1.3 Marangoni convection

Marangoni convection can be introduced as a flow through an interface due to local surface tension gradients [9]. The gradients can be resulted from alteration in temperature, concentration or electrical potential [10]. As a result, a movement in the interface is observed from the region with lower surface tension to higher one. The movement boosts heat and mass transfer along the interface in these regions [11]. The interface forming between liquid-liquid or gas-liquid is termed the Marangory boundary. Marangoni convection is observed in many areas including the expansion of vapor baloons arised from temperature or solutal gradient, analysis of fluid behavior in the systems under microgravity [12]. In addition, this phenomenon can be significant for small scale systems. Gravity forces are negligible due to little amount of the fluid in the system. Thus, surface tension forces can become the driving force for the system [13]. Marangoni effect is interpreted in literature with a dimensionless number, Marangoni number (Ma) which contributes to understanding the relation between surface tension gradient resulted from change in temperature gradient and viscous force. Higher Marangoni number means higher Marangoni forces via the gradient in surface tension [14].

1.1.4 Wetting

Wetting is an ability of a liquid to spread on a solid or liquid substance [15]. To represent the wetting properties of flat and rough surfaces, an angle is drawn where a liquid/vapour surface contacts with solid surface like in Figure 1.4.

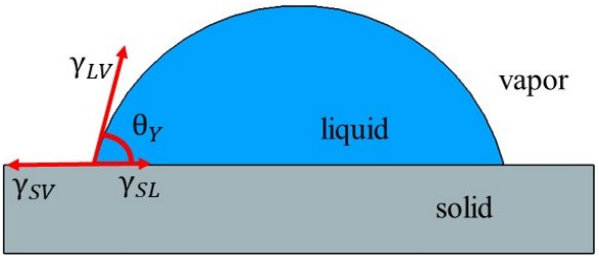

Figure 1.4: The schematic representation of the contact angle, adapted from [16]

The mentioned angle is named "contact angle" and is calculated based on the mechanical equilibrium, as presented in Eqn. 1.4 of the system in Figure 1.4 under the influence of three interfacial tensions including solid-liquid, solid-vapour, and, liquid-vapour.

$$\gamma_{LV} cos\theta_Y = \gamma_{SL}\gamma_{SV} \tag{1.4}$$

where ,γ_{SL}, γ_{SV} and γ_{LV} refers to the interfacial tensions of solid-liquid, solid-vapor, and liquid-vapour, respectively. When Eqn. 1.4. is noted Young's equation, θ_Y indicates Young's contact angle [17]. Wenzel and Cassie–Baxter models provide information about how a static water contact angle can be raised by altering surface roughness in homogeneous and heterogeneous wettings [18].

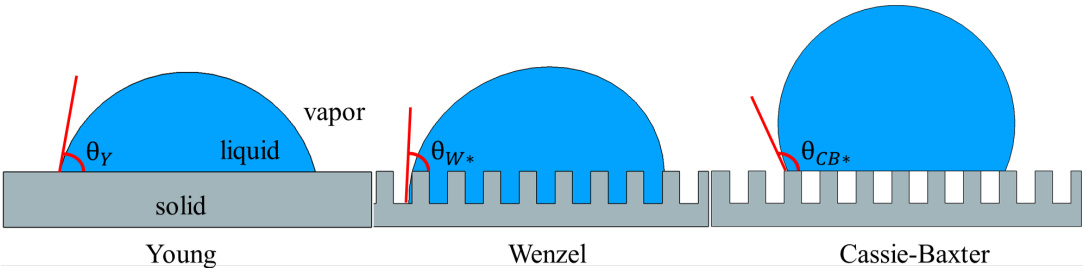

Figure 1.5: The contact angles for different wetting states in textured structures, adapted from [18]

In Wenzel's model, the grooves of the roughened surface are filled entirely by the

liquid. Therefore, the area of the interface between water and liquid increases. On the other hand, in Cassie-Baxter State, the contact area between water and solid is minimized via causing water to form spherical droplets due to the structure with hydrophobic characteristics [18]. Both states can be reviewed in Figure 1.6.

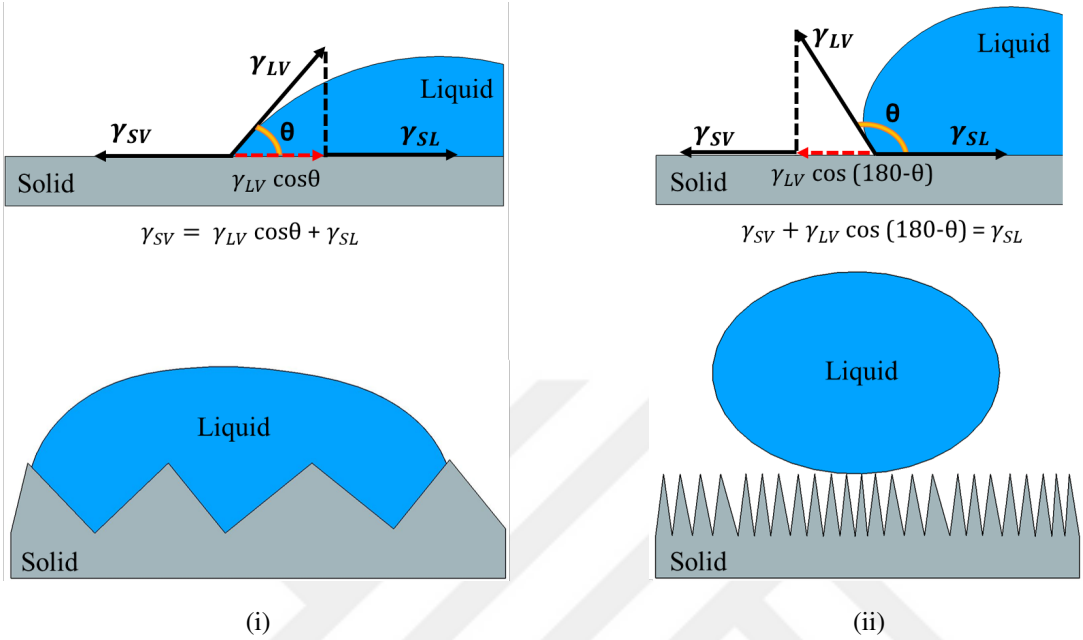

Figure 1.6: (i) Wenzel and (ii) Cassie-Baxter State in roughened surfaces [19]

1.2 Literature Review

Marangoni convection is defined as a motion of heat and mass at the interface due to local gradient in the interfacial tension. The gradient can occur owing to variation of solute concentration, temperature or electrical charge at the interface [20].

In the terminology of literature, when the interfacial tension is frequently termed as surface tension for the gas/liquid interfaces [21], the particular statement observed by temperature gradient is termed thermo-capillary convection or Bénard–Marangoni convection [22].

The phenomenon has been examined in various-scale systems including nano [23], micro [24, 25] and macro scales [26] based on continuous phase flow. Moreover, there has been some researches about Marangoni behavior in droplets. In the study

of Chen et al. [27], the efficiency of mass transfer and the morphology of droplet are examined by parallel visualization experiments. Arendt et al. [28] analyzed the effect of surfactant on mass transfer in the system water–acetone–toluene in terms of various solute concentrations in the droplet. Using this behavior driven by solutal gradient, Park et al. [29] proposed an innovative method to increase the efficiency of mixing within a droplet with Marangoni effect. In terms of Marangoni convection in microgravity environment, the flow behavior in large-scale liquid bridge, comprising of two disks with different temperature, are remarked for various studies. Taishi et al. [30] and Koichi et al. [31] conducted the experiments for the system with liquid bridge on the International Space Station in microgravity environment. As a result of these experiments carried out, Marangoni instability as well its effect on heat transfer at the liquid-gas interface were observed in terms of high Prandtl number liquids.

In the literature review, there has been the considerable number of the studies for systems open to atmosphere. Especially, the systems like in lid-driven cavity problem have been examined comprehensively. For instance, the study of Cicek et al. [32] reviewed the behavior of the thermo-capillary flow exposing temperature gradient in the square cavity in terms of Rayleigh and Marangoni numbers. Another study conducted by Biswas et al. [33] discussed this problem via taking account of more than one factor including temperature as well as magnetic field effects. Based on a different approach, Hartmann number providing the comparison between magnetic and viscous forces was evaluated with Marangoni number under the same study.

As for the Marangoni-induced flow in the closed systems with internal flow, the study of Zhenchen et al. [34] numerically constructed a closed micro cavity system with binary fluids using both temperature and pressure gradient as a motion inducer. Amador et al. [35] represented a novel micro pump induced by temperature gradient occurring at the interfaces between the working fluid and air naturally remaining after the water was injected to the system. The case in which the air intrinsically remains in the cavity of the micro pump reveals another phenomenon called Cassie-Baxter state. The Cassie-Baxter state is a surface wetting phenomenon that elucidates the relation between the surface tension and Young's contact angle in a channel made of hydrophobic material like polydimethylsiloxane (PDMS) [36]. Utilizing the assumption that the water does not fill the cavity because of the Cassie-Baxter state, water flow in a microchannel was investigated numerically and analytically for a two-

dimensional system in the study of Tobias et al. [37]. The study representing creeping flow analysis utilized temperature gradient as the driving force. On the other hand, Cassie-Baxter state analysis have been used for various aims. Namely it takes place in a review study of Hanaei et al. [38] in terms of self-cleaning due to hydrophobicity. Moreover, the study of Darmanin et al. [39] inquries the hydrophobicity in nature via Cassie-Baxter phenomenon analysing fluid behaviour on the wing of insects or the leaves of the plants. Furthermore, the study of Mall et al. [40] investigated a textured microchannel in terms of different geometric conditions. As a consequence, decrease in pressure drop is obtained as the size of Marangoni boundary is increased.

All analysis about the hydrophobicity is related with the material of the structure. In this point, polydimethylsiloxane (PDMS) having hydrophobic characteristic gains importance due to its good physical properties. It has high tensile modulus (1.8 MPa), low thermal conductivity such that can be used in an insulated study, good gas permeability, transparency providing to detect reactions during studies, high elongation (160 %), thermally stability below 423.15 K. In addition to them, its fabrication is easy in even micrometric sizes via molding [41]. Due to the goodness in its properties, Tayyaba et al. [42] and Le et al. [43] conducted the studies about the PDMS fabrication for biomedical application and micro-valve system, respectively. In microfluidics, usage of polydimethylsiloxane (PDMS) in microfluidics is cited as a revolution and the age has been called PDMS age due to its excellent characteristics and contributing easiness to construct the experiments [44].

1.3 Motivation of Thesis

Microfluidic systems have drawn attention due to their applications in various fields such as space and biological systems, and cooling systems in micro devices. For small scale problems, gravity is negligible; therefore, the analysis of other forces, such as surface tension, is of great importance [13]. Marangoni convection can be defined as the movement through interface between two fluids due to the gradient of surface tension. This gradient stems usually from the local change in temperature or concentration [5].

To the literature survey, there has been relatively a few studies in terms of Marangoni

convection in the closed vertical systems and the temperature gradient's effect in Cassie-Baxter state occurring in the system with hydrophobic characteristic. As some reasons underlying of this situation, it can be said that the systems open to atmosphere already have a fluid-fluid interface with air. However, to form interfacial surfaces between fluids in the closed systems requires extra analysis whether capillary or adhesive forces dominates interfacial forces. As for Cassie-Baxter state, the investigations generally have targeted to decide the contact angle or analysis the flow in terms of the pressure effect rather than temperature effect. On the other side, Marangoni-induced flow in a system provides a motion without pumping in the region under Cassie-Baxter state that indicates intrinsically an interface between air and fluid. Moreover, it can be used for flow control with only creating surface tension gradient in especially microfluidics [45]. Furthermore, it can be a solution for the problem about great pressure drop in microfluidics induced by pumping. Marangoni boundary having slip-condition improves the pressure drop in the system [40].
To sum up, a gap is observed for the analysis of thermo-capillary flow in a vertical textured microchannel under Cassie-Baxter state. Also the factors created for Marangoni flow can be a solution for the problems in microfluidics like pressure drop. Thus the topic of the thesis is chosen in this area.

1.4 Thesis Aim and Outline

In this study, two phenomena, Marangoni effect and Cassie-Baxter state, are coupled. After validating the horizontal system constructed to compare with the experimental study of Amador et al. [35], the targeted vertical configuration is focused on. The pressure at the inlet of the vertical system is higher due to its height. Thus Cassie-Baxter state is used to determine the critical pressure at which the water cannot enter the cavity. The aim of the present numerical work is to characterize Marangoni-induced flow occurring due to wetting property of PDMS in vertical microchannels having air-filled cavities. Marangoni effect is established via temperature gradient between inlet and outlet. The analysis is carried out with different geometric conditions for the microchannel. Therefore, the dominancy of two forces of surface tension and gravity are observed and reported by taking account of Cassie-Baxter state.

In Chapter 1, firstly general information is given about microfluidics, Marangoni phenomenon and the topics related them. Then the studies carried out are elaborated in literature review. Based on the information or gap in literature, the reasons why the topic is selected for thesis are presented. The aim and brief summary of thesis are mentioned.

In Chapter 2, a thorough definition for the system in the thesis is done. Model configurations, tables including parameters and boundary conditions of the system are presented. After mesh independence study is explained, parametric study is constructed.

In Chapter 3, the physics of simulation is validated via the experimental studies in the study of Amador et al. [35]. Then the system is tested by the conditions resulted from Cassie-Baxter state. After validating, the targeted simulations are concentrated on. Temperature variation, velocity magnitude, and the flow structure inside the channel are investigated for various sizes of parameters values based on Marangoni number.

In Chapter 3, a validation study is performed for a horizontal microchannel. The results are compared to the experimental data in the study of Amador et al. [35].

In Chapter 4, after the physics that introduces Marangoni effect into the system is ensured by the validation study, a parametric study for the targeted vertical microchannel is conducted. Thus, Marangoni effect is investigated in terms of different dimensions of the vertical microchannel for different temperature differences between inlet and outlet.

In Chapter 5, the results are summarized via brief comments. The relation between parameters and output are discussed in a general approach. Future work is recommended.

CHAPTER 2

METHODOLOGY

2.1 Model Configuration

The current investigation examines Marangoni effect on the flow characteristic, temperature and velocity profiles in a vertical microchannel. The closed straight microchannel is made of polydimethylsiloxane (PDMS). It has front and back walls and equal-sized air cavities only in the right and left sides, observed in Figure 2.1. To the front view, the mid-plane of microchannel is given in Figure 2.2i and its 3D schematic exception front and back walls is presented in Figure 2.2ii. W, d and L refers the width, depth, and length of water in the microchannel and a, b, c denote the height, width of the cavity, and the height of single solid partition that contacts with the water in the microchannel, respectively.

The height of the cavity (a) is 100 μm. It is small enough to avoid water penetration due to Cassie-Baxter condition that occurs in the textured microchannel made of hydrophobic material like PDMS. As mentioned in Section 1.1.4, this surface phenomena is observed in the interface between the water and air because of the relation between surface tension and Young's contact angle [36]. Thus, an interface between water and air occurs on air-water interface in Figure 2.2ii and the fluid is assumed to be single phase. The air in the cavity is taken into account in the boundary for air-water interface. The system utilizes surface tension in these boundaries to drive the fluid. As discussed in Section 1.1.2, surface tension is a function of temperature. Therefore, a temperature difference of ΔT between inlet and outlet is applied to the microchannel to form a local surface tension gradient. The fluid flow in the microchannel is investigated for various geometrical parameters and for different temperature gradients as given in Table 2.1. The temperature is taken as 305 K.

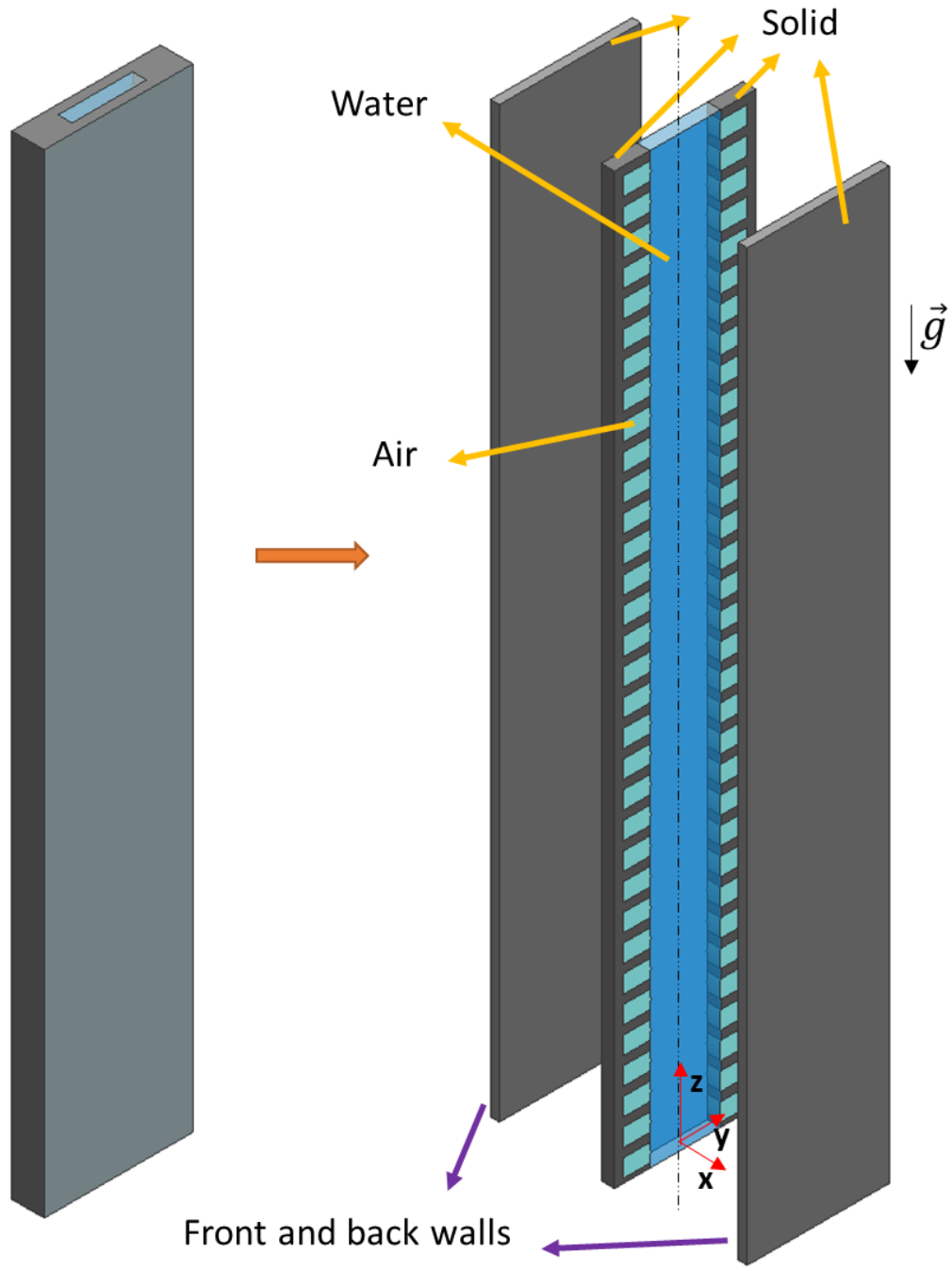

Figure 2.1: 3D view of a vertical microchannel

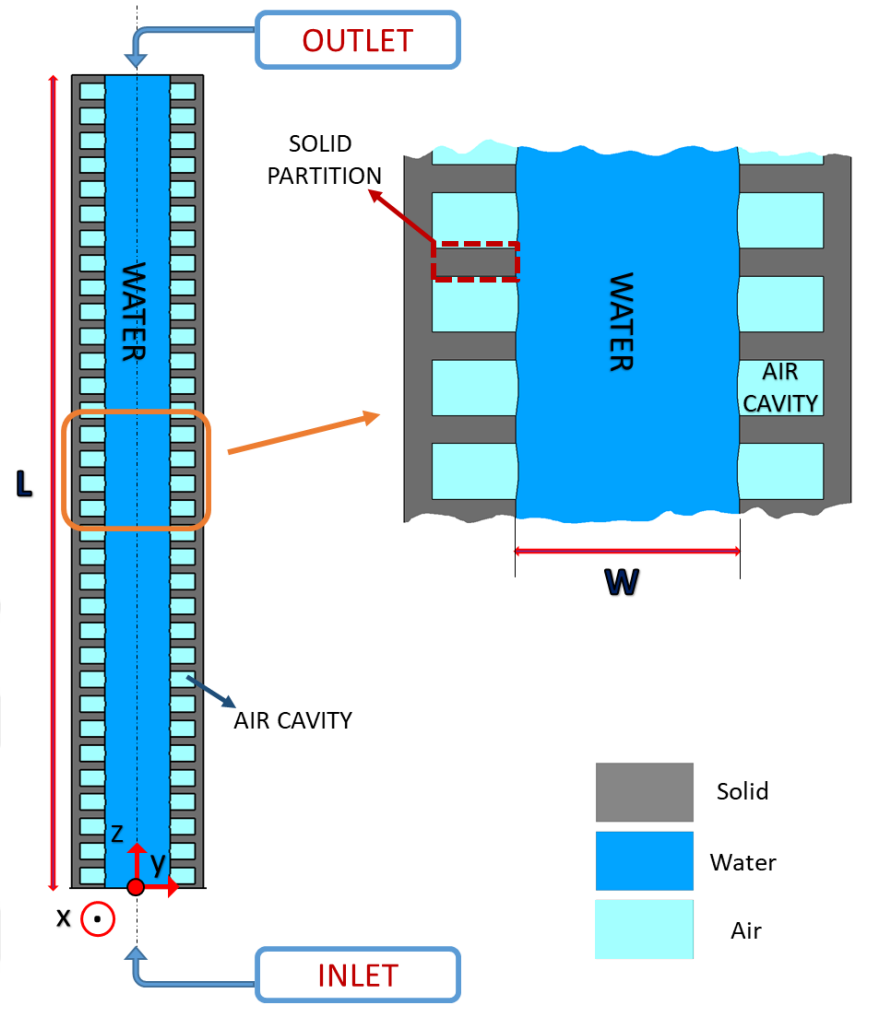

(i) YZ mid-plane

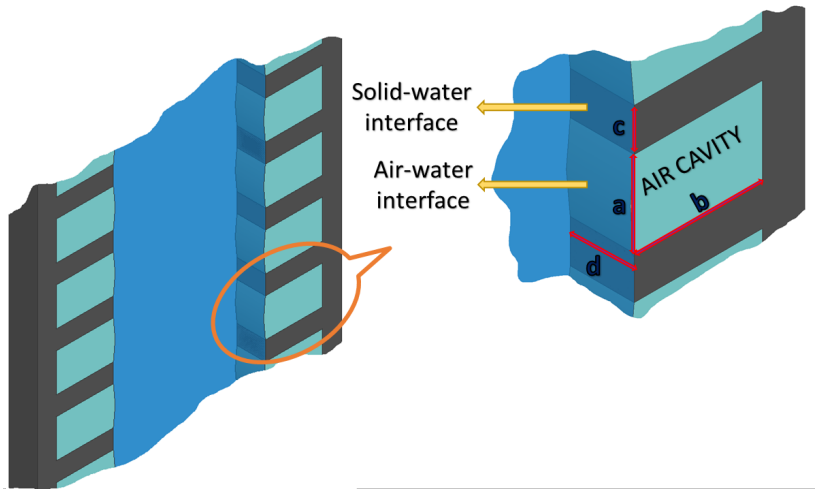

(ii) Dimension representation

Figure 2.2: Schematic illustration of a vertical microchannel

Table 2.1: Geometrical parameters of the vertical microchannel

Parameters	**Values**
Air cavity height (a) [μm]	100
Air cavity width (b) [μm]	150
Solid partition height (c) [μm]	25, 50, 100
Water width (W) [μm]	400, 800, 2000
Water depth (d) [μm]	75, 150, 300
Vertical microchannel length (L) [μm]	5000

2.2 Computational Domain

The actual vertical microchannel includes identical air cavities between solid partitions the number and the position of which in the z-direction are the same due to symmetry at the xz plane. However, the numerical model does not mathematically solve the air domains and assumes a shear boundary condition due to Marangoni effect at the water-air interface. The solid domain with the thickness of s is neglected since the air domain is not modeled. Because the PDMS has a low thermal conductivity value, in order to observe the solid temperature gradients in the x and y directions, two walls with a thickness of 50 μm are placed at $x = \mp d/2$. Figure 2.3 shows the details of the numerical domain used in this study. The water-air and water-solid interfaces are shown in Figure 2.3. The details of the boundary condition are given in the following section. Due to geometrical symmetry and to save computational costs and time, half of the microchannel is modeled as depicted in Figure 2.3. The numerical domain is created in COMSOL 5.6 Multyphysics.

The fluid is assumed to be single phase as mentioned from the reasons in Section 2.1. The governing equations include continuity, momentum and energy equations for the water domain and only the conduction equation for the solid domain.

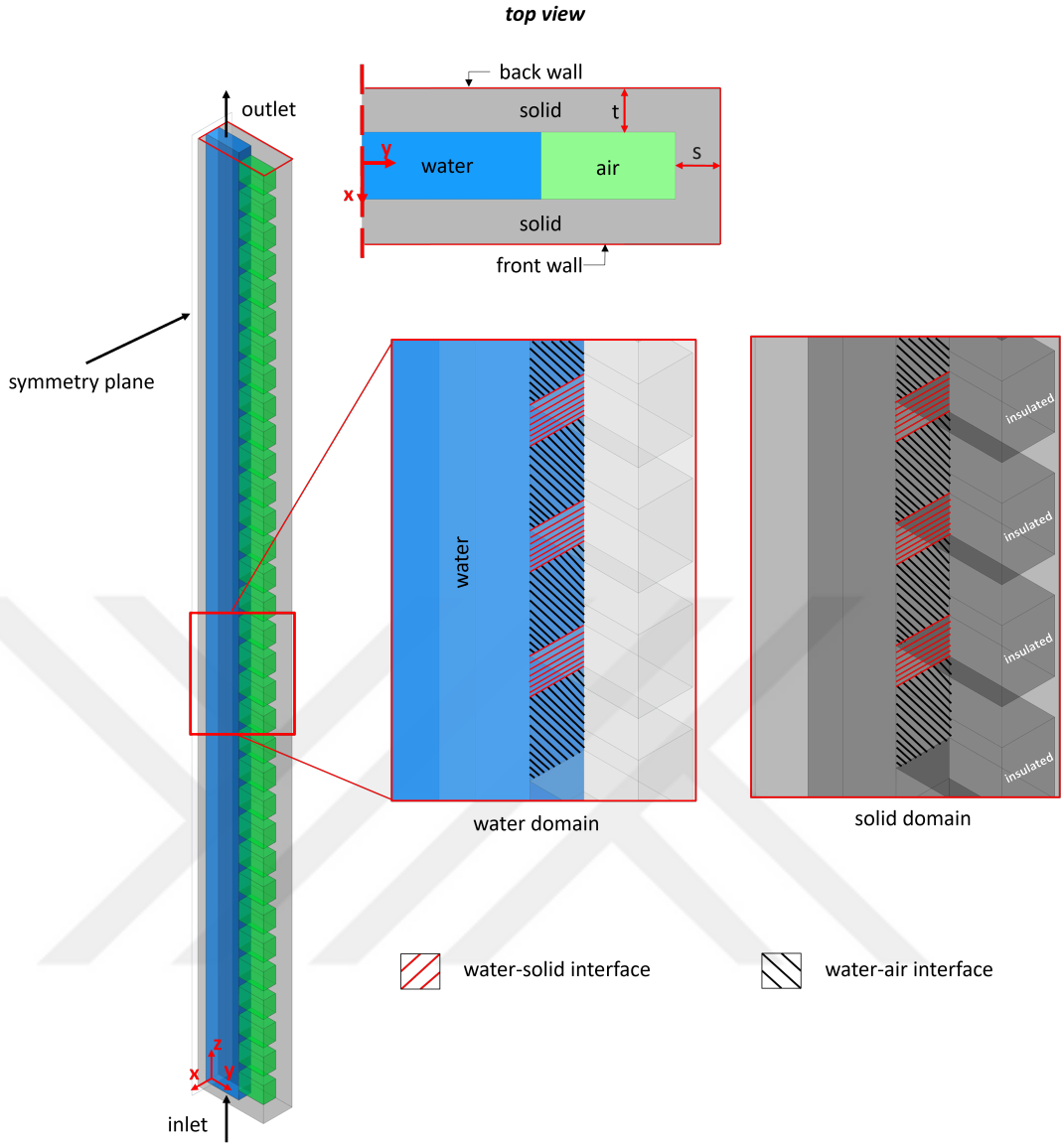

Figure 2.3: Schematic illustration of the computational domain

2.3 Boundary Conditions

2.3.1 Inlet and outlet

The inlet at $z = 0$ and outlet at $z = L$ of water domain in microchannel as given in Figure 2.3 are open to the atmosphere ($P = 0$) and their temperatures are set to constant values of $305 + \Delta T/2K$ and $305 - \Delta T/2\ K$, respectively.

2.3.2 Solid-water interface

At the interface between solid and water domains, no-slip condition is applied. Additionally, the temperature and heat flux are equal to resolve the continuous behavior of the temperature field.

2.3.3 Water-air interface

In order to model the Marangoni effect, two shear stress terms are defined as given in Eqn. 2.1 and Eqn. 2.2 [33]. It is important to note that the height of the air cavity (a) is selected such that no water can penetrate into the air domain based on the benchmark study [35].

$$\tau_{yx} = -\frac{\delta\sigma}{\delta T}\frac{\delta T}{\delta x} \tag{2.1}$$

$$\tau_{yz} = -\frac{\delta\sigma}{\delta T}\frac{\delta T}{\delta z} \tag{2.2}$$

In equations 2.1 and 2.1, σ, μ ,T and V_z are the surface tension, dynamic viscosity, temperature and the velocity in z-direction, respectively. τ_{yx} and τ_{yz} denote the shear stresses in x-direction and z-direction acting on the plane normal to the y-direction, respectively. The fluid is assumed to be Newtonian therefore the shear stress terms can be written as:

$$\tau_{yx} = \mu\frac{\delta V_z}{\delta z} \tag{2.3}$$

where V_z is the velocity in z-direction. If the shear stress expression in the Eqn. 2.3 is substituted into Eqn. 2.1 and Eqn. 2.2, the equations in Eqn. 2.4 are obtained.

$$\tau_{yx} = -\frac{\delta\sigma}{\delta T}\frac{\delta T}{\delta x}, \tau_{yz} = -\frac{\delta\sigma}{\delta T}\frac{\delta T}{\delta z} \rightarrow \mu\frac{\delta V_x}{\delta x} = -\frac{\delta\sigma}{\delta T}\frac{\delta T}{\delta x}, \mu\frac{\delta V_z}{\delta z} = -\frac{\delta\sigma}{\delta T}\frac{\delta T}{\delta z} \tag{2.4}$$

Eqn. 2.4 is converted into the non-dimensional form by introducing the non-dimensional variables in Eqn. 2.5:

$$\Omega = \frac{V_z a}{\alpha}, Z = \frac{z}{a}, \Phi = \frac{T - T_s}{\Delta T} \tag{2.5}$$

σ, α are the surface tension and water thermal diffusivity, respectively. After non-dimensionalizing, the expression in Eqn. 2.6 is obtained.

$$\frac{\delta\Omega}{\delta z} = -\frac{\delta\sigma}{\delta T}\frac{\Delta T a}{\alpha\mu}\frac{\delta\Phi}{\delta z} \tag{2.6}$$

Based on the expression in Eqn. 2.6, Marangoni number mentioned in Section 1.1.3 is obtained via the coefficient of non-dimensional variables, given in Eqn. 2.7:

$$Ma = -\frac{\delta\sigma}{\delta T}\frac{\Delta T_m a}{\mu\alpha} \tag{2.7}$$

where ΔT_m is temperature difference through the height of the air cavity on the water-air interface exposed to Marangoni effect. In the parametric study, Marangoni number presenting relation between surface tension and viscous forces [46] is evaluated for each air cavity to interpret the results. The derivation of surface tension is obtained by Eqn. 1.1. μ, α are found via interpolating the properties at the table provided by Cengel and Cimbala [47].

The outer surfaces of the front and back walls are assumed to be insulated. Also, since the air in the cavity is not numerically modeled, the surfaces touching the cavity and solid partitions (at $y = W/2 + b$) are insulated.

2.4 Governing Equations

It is stated that no-slip and continuum assumptions can be applied for the flow if Knudsen number of the flow in the vertical microchannel is less than 0.001. Knudsen number can be expressed in the Eqn. 2.8,

$$Kn = \frac{\lambda}{L_c} \tag{2.8}$$

$$L_c = \frac{4A_c}{P_{wetted}} = \frac{4Wd}{2(W+d)} \tag{2.9}$$

where λ, L_c, A_c, and P_{wetted} refer to the mean free path, characteristic length, cross-sectional area, wetted perimeter, respectively.

Mean free path length refers the average distance a particle moves before collisions. For water, it is accepted almost 0.31 nm [48]. In a conservative approach, the minimum values of width (W), 400 μm, and depth (d), 75 μm, of the water in vertical microchannel are used for the calculation of Knudsen number. As a result, the characteristic length (L_c) of the microchannel is evaluated almost 126 μm and then Knudsen number is calculated as $2.5 \cdot 10^{-6}$. Therefore, continuity, momentum, and energy equations in Eqn. 2.10 to Eqn. 2.12, respectively are used with the assumptions of

steady state, being incompressible and no heat generation:

$$\nabla \cdot \vec{V} = 0 \tag{2.10}$$

$$\rho(\vec{V} \cdot \nabla)\vec{V} = \rho\vec{g} - \nabla P + \mu\nabla^2\vec{V} \tag{2.11}$$

$$\nabla \cdot (k\nabla T) = \rho C_p \vec{V} \cdot \nabla T \tag{2.12}$$

where $\vec{V}$, ρ, $\vec{g}$, P, μ, C_p T, k are the velocity vector, density of the water, gravity vector, pressure, dynamic viscosity, specific heat capacity, temperature and thermal conductivity, respectively. The system is steady state so the variables do not depend on the time change and some terms are dropped due to $\frac{\delta}{\delta t} = 0$. Moreover the characteristic of PDMS is taken in consideration to apply Cassie-Baxter state that explains the fluid behavior in the hydrophobic microchannel having air cavities.

2.5 Computational Methodology

Simulations are performed in COMSOL Multiphysics 5.6 based on the Finite Element Method (FEM). The whole domain is discretized into the smaller sections termed elements. True solution is approximated using the shape functions, that can be defined with different orders, in each element. If linear, first order, shape functions are used for both velocity and pressure in a simulation of fluid flow, this is called P1+P1 in FEM [49]. In the thesis, P1+P1 is used for velocity and pressure fields. Higher order terms are usually recommended for simpler flow types such as creeping flow since the solution is not complicated compared to laminar flow with diffusion and convection terms. Also linear discretization is used for the temperature field. All equations are solved in a coupled way with PARDISO scheme, a direct solver, due to its convenient speed.

2.5.1 Input parameters

The data about water and surface tension of water-air is obtained by COMSOL Library, whereas the data about surface tensions of silicon oil-water and dodecanol-water is integrated into the simulation manually via Eqn. 1.2 and Eqn 1.3. On the other hand, the PDMS properties [50] in Table 2.2 and the values of temperature

difference (ΔT) between inlet and outlet, including 0.2, 0.8, 1.7, 3 K, are used in modeling.

Table 2.2: PDMS properties

Properties	**Values**
Heat capacity [$kJkg^{-1}K^{-1}$]	1.5
Density [kgm^{-3}]	970
Thermal conductivity [$Wm^{-1}K^{-1}$]	0.15

2.6 Mesh Independence Study

The system is in micro-scale and viscous forces are significant through the whole vertical microchannel. Thus, specific sizing is not used for the boundary layer that is defined in the region near wall [47] due to large boundary layer thickness. Therefore, a uniform structured mesh is utilized for the water domain. Figure 2.4 depicts a typical element used in the water domain.

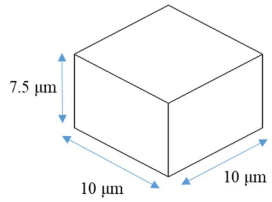

Figure 2.4: A typical element inside the water domain

For the solid domain, coarser unstructured elements are used since in the solid domain, only the conduction equation which is a Laplace equation is solved that does not require high-resolution meshes. The solid domain meshes are set to get larger towards the y-direction with a specific growth rate that resulted in minimum element quality ranging between 0.18 and 0.20. General mesh structure is shown in Fig 2.5. The same mesh density is applied to other cases.

After checking quality, mesh independence study is carried out using the channel with the smallest dimensions. As given in Table 2.3, five different mesh studies are done.

For the studies, a computer using Intel(R) Xeon(R) CPU E5-1620 0, with 4 cores and 8 logical processors is used.

Table 2.3: Mesh properties and mesh independence study results

	Number of elements	**Average velocity ($\bar{V_z}$) in z direction [μms^{-1}]**	**Run time [min]**	**Difference in $\bar{V_z}$ [%]**
Mesh 1	31952	25.59	7	18.8
Mesh 2	80336	28.42	27	9.97
Mesh 3	170098	29.58	85	6.12
Mesh 4	299250	30.35	217	3.7
Mesh 5	1061690	31.51	6455	-

Average velocity in z-direction ($\bar{V_z}$) is taken as the parameter to study the mesh independence. The difference in percent with the finest mesh is calculated and given in Table 2.3. Run time in the simulation with Mesh 5 is out of practical range. Thus Mesh 4 having relatively reasonable difference compared to Mesh 5 is chosen.

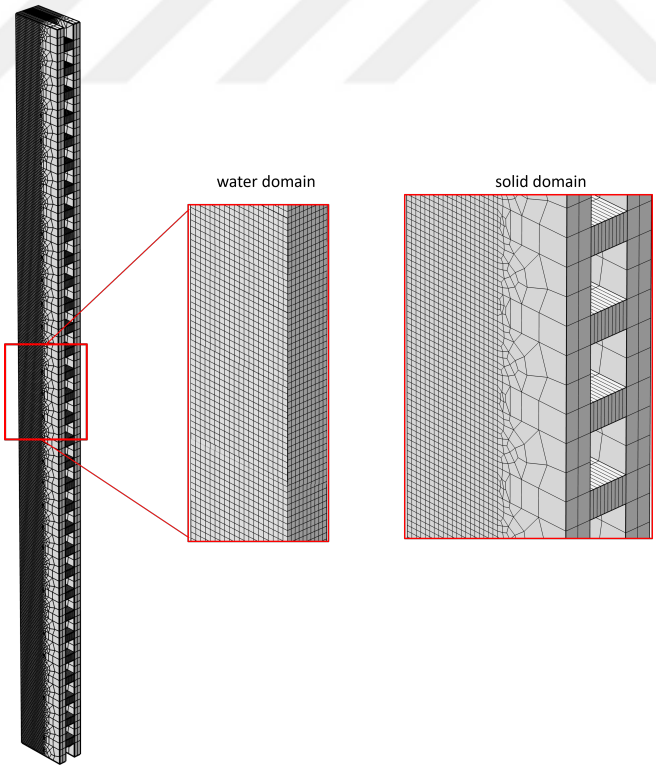

Figure 2.5: Meshing configuration of the computational domain

2.7 Parametric Study for Vertical Microchannel

The effects of the water depth (d) and width (W), the height (c) of single solid partition that contacts with the water in the microchannel, and temperature difference (ΔT) between the inlet and outlet of the microchannel on the thermal and hydrodynamic behaviors are studied as a parametric study.

In this study, the length (L) of the microchannel is accepted to be a constant. Thus when the size of the solid partition height (c) changes, only the number of the cavities increases. To increase the size of the height (a) of the cavity requires a comprehensive approach including Cassie-Baxter state that the surface tension is more prominent against capillary forces. The more the sizes of the cavity width increases, the more the fluid would be driven into the cavity by capillary forces [51]. As a result, the water can penetrate the cavity. This leads to turn the system with one phase into with two phases. Accordingly, the system dynamics is likely to alter. Thus it is taken as a constant. Changing the width of the cavity (b) does not contribute to fluid flow characteristics. The knowledge about its size is necessary for satisfying the state that the water droplet should not touch inner wall of the cavity. It can be shown by the condition in Eqn. 2.13[40],

$$\frac{b}{a} > -\frac{1 - 2\sin\theta_Y}{2\cos\theta_Y} \tag{2.13}$$

where θ_Y is Young's contact angle in Figure 2.6.

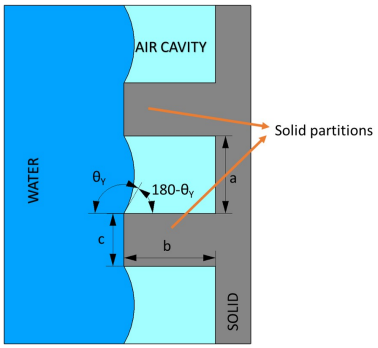

Figure 2.6: Young's contact angle for the vertical microchannel

The critical depth (b) of the cavity is calculated as almost 128 μm for the microchannel. In the case of lower values than 128 μm, adhesive forces will dominate surface tension and the cavity will fill with water. In this analysis, the width of the cavity

is accepted 150 μm. Thus the condition that the water should not penetrate into the cavity is satisfied in terms of physical configuration. Based on the aforementioned information, the parametric analysis is performed for the parameters in Table 2.1 for different temperature difference values including 0.2, 0.8, 1.7, 3 Kelvins.

CHAPTER 3

VALIDATION STUDY

A validation study for a horizontal microchannel is constructed to replicate the experimental results of Amador et al. [35].

The horizontal PDMS microchannel in the experimental setup has the cavities filled with air. Driving force is the Marangoni-induced shear stresses occurring at the interfaces between air and water due to temperature difference, which is created by Peltier devices. The schematic of the experimental horizontal microchannel is given in Figure 3.1. The geometrical conditions and corresponding working fluids used in the experimental study are summarized in Table 3.1.

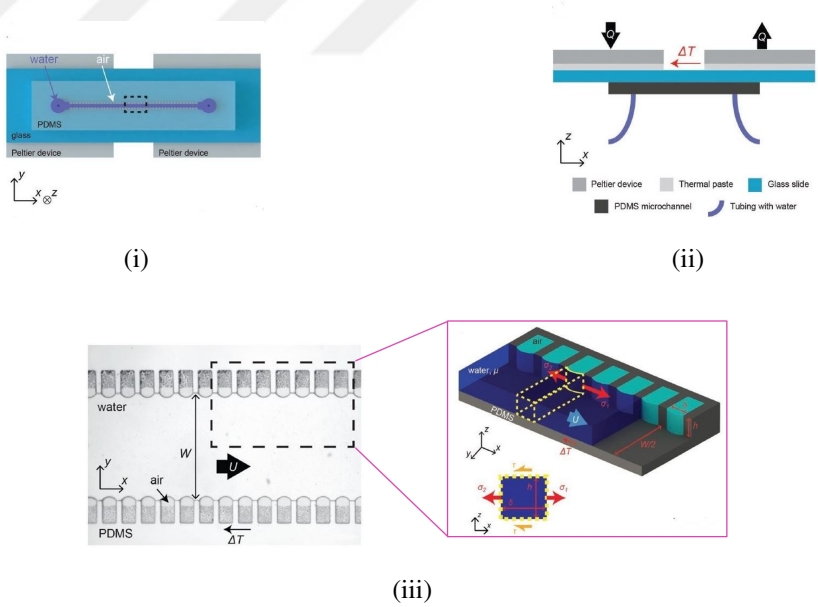

(i) (ii)

(iii)

Figure 3.1: Illustration of experimental setup in the study of Amador et al. [35] (i) top, (ii) side, and (iii) detail views

Table 3.1: Validation cases

Cases	**Working fluid**	**Solid partition height (c) [μm]**	**Water width (W), depth (d), and length (L) [μm]**	**Temp. difference (ΔT) [K]**
1	Water	75	400, 75, 10000	0.2, 0.8, 1.7, 3
2	Water	75	700, 75, 10000	0.2, 0.8, 1.7, 2.3
3	Water	75	900, 75, 10000	0.2, 0.8, 1.7, 2.3
4	Silicon oil	75	700, 75, 10000	-0.2, -0.8,-1.7, -2.3
5	Dodecanol	75	700, 75, 10000	-0.2, -0.8,-1.7, -2.3

As presented in Figure 3.2 and Figure 3.3, the average velocity is directly proportional to temperature difference for both experimental and validation studies performed using four different temperature differences (ΔT). A linear curve is fit to the results obtained via the validation study to show the linear relationship. Based on the line, the mean absolute errors are calculated like in Table 3.2. On the other hand, the dotted line in the graphs depicts the line fitted to the experimental results, taken from the study of Amador et al. [35].

Table 3.2: Absolute errors between [35] and validation study

Validation cases	**Absolute error [$\%$]**
Case 1	31.4
Case 2	35.0
Case 3	30.0
Case 4	22.8
Case 5	25.4

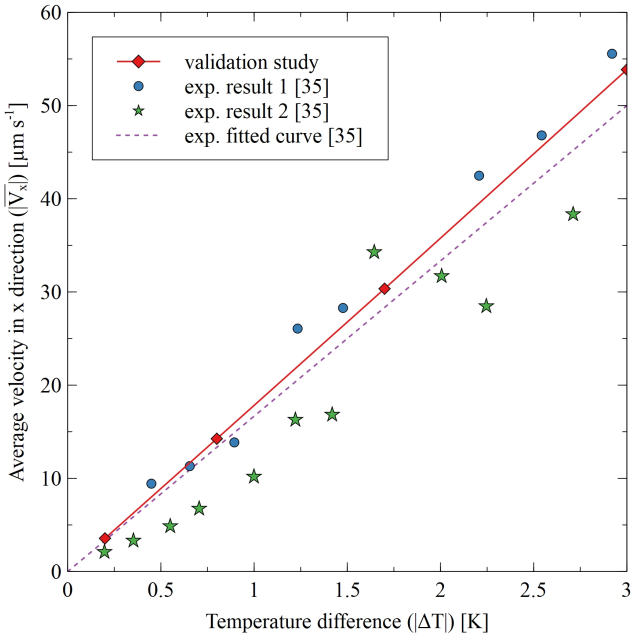
validation study
exp. result 1 [35]
exp. result 2 [35]
exp. fitted curve [35]
Average velocity in x direction ($|\overline{V_x}|$) [μm s^{-1}]
Temperature difference (|ΔT|) [K]
0
10
20
30
40
50
60
0
0.5
1
1.5
2
2.5
3

(i)

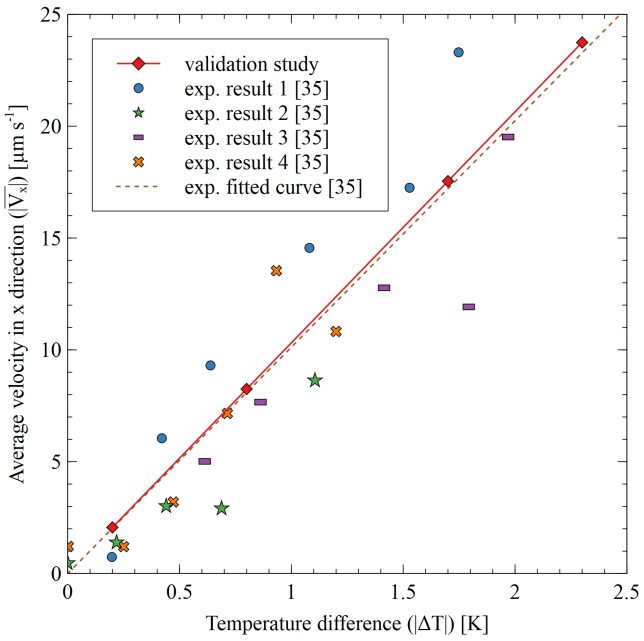
validation study
exp. result 1 [35]
exp. result 2 [35]
exp. result 3 [35]
exp. result 4 [35]
exp. fitted curve [35]
Average velocity in x direction ($|\overline{V_x}|$) [μm s^{-1}]
Temperature difference (|ΔT|) [K]
0
5
10
15
20
25
0
0.5
1
1.5
2
2.5

(ii)

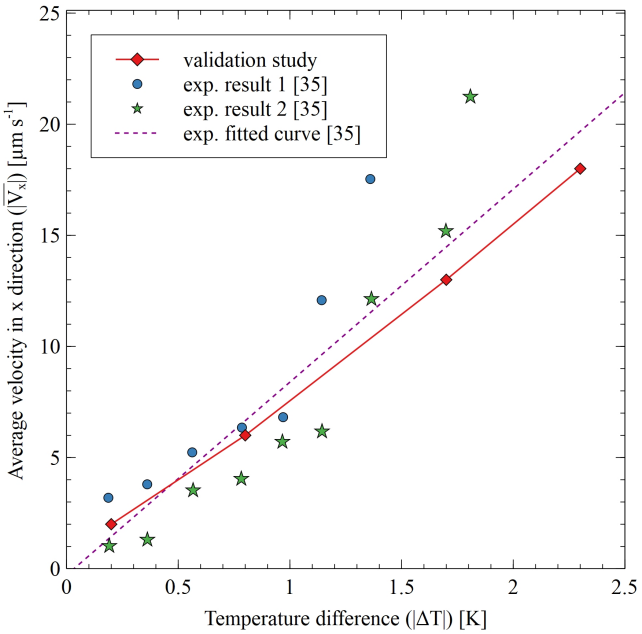

(iii)

Figure 3.2: Comparison of numerical results with [35], for water width (W) of (i) 400 μm (ii) 700 μm (iii) 900 μm

The values of velocity and temperature in the plots are shown as an absolute value since the relation between the surface tension and temperature changes for each fluid. With an increase in temperature, the surface tension of water decreases; however, the surface tension of silicon oil and dodecanol increases. Therefore, for the sake of cohesiveness, the absolute value of velocities is used in the figures.

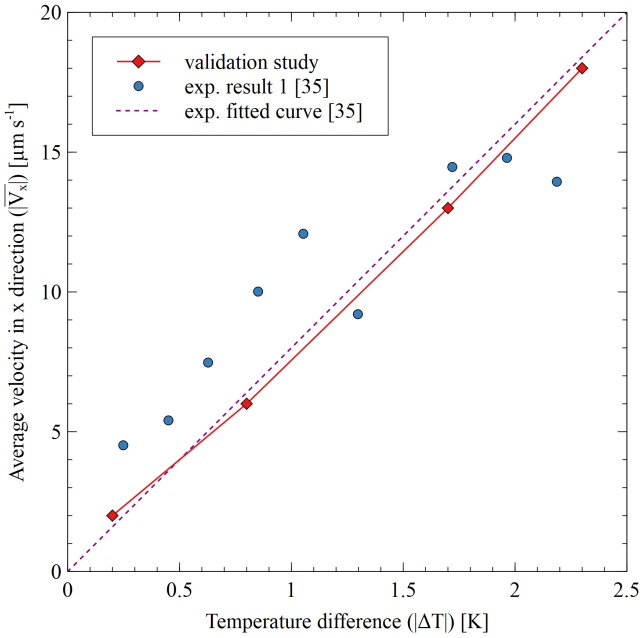

(i)

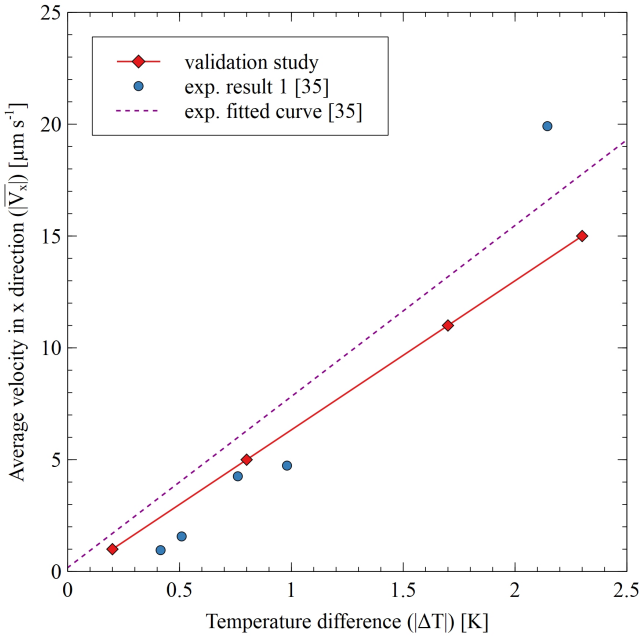

(ii)

Figure 3.3: Comparison of numerical results with [35] for (i) silicon oil and (ii) dodecanol

The validation study is performed for various geometrical conditions including different microchannel sizes, with the width of 400 μm, 700 μm and 900 μm for various types of working fluid; water, dodecanol and silicon oil.

As demonstrated via the dotted line in the study of Amador et al. [35], experimental results refers to a linear behavior. In line with this, the linear curve fitted to validation study results shows a linear behavior and its inclination matches with the inclination of the dotted line exception dodecanol as depicted in Figure 3.2 and Figure 3.3.

For the dodecanol as the working fluid, only the last experimental data creates a deviation when compared to the numerical model which might be due to a mistake in measurement.

In general, the validation study results are found in good agreement with experimental results in the study of Amador et al. [35] because of matching the general inclination of the output.

CHAPTER 4

PARAMETRIC STUDY FOR THE VERTICAL MICROCHANNEL

4.1 Parametric Computational Analysis

After validating the numerical results in the horizontal microchannel with experimental results presented by Amador et al. [35], this chapter of the thesis deals with the vertical microchannel with a parametric study, numerically. Since the vertical microchannel has a larger height, the pressure occuring in its inlet is greater than the horizontal configuration. Thus, as elaborated in Section 1.1.4 the critical pressure, P_c, representing the threshold for wetting transition from Cassie-Baxter to Wenzel state [36] is estimated for this microchannel. It is important to test whether the water penetrates into the air cavities or not when the microchannel turns from horizontal to the vertical orientation,

$$P_c = -\frac{4\gamma_{LV} f \cos\theta_Y}{(1-f)a} \tag{4.1}$$

where γ_{LV} is the vapor-liquid interfacial tension, f is the fraction of solid on apparent wetted area [36], θ_Y is the Young's contact angle. The variable f can be defined as the ratio of water-solid interface area to the total area that water touches in one cavity depicted in Figure 2.2ii and is given in Eqn. 4.2 as:

$$f = \frac{cd}{(a+c)d} \tag{4.2}$$

As noticed in Eqn. 4.2, the water depth (d) does not effect the fraction (f). The height (a) of the cavity is constant as mentioned in Section 2.1. As for the solid partition height (c), the size of 25 μm is used in a conservative way so that all parametric cases can be satisfied. The maximum pressure that satisfies Cassie-Baxter condition is calculated to be almost 242 Pa by Eqn. 4.1 for 5000-μm-long vertical microchannel with the values provided in Table 4.1.

Table 4.1: Model parameters

Parameters	**Values**
vapor-liquid interfacial tension (γ_{LV}) [N μm^{-1}]	70.72x10^{-9} at 305 K [7]
Young's contact angle (θ_Y) [°]	$\approx$ 110 for water-PDMS [36]
air cavity height (a) [μm]	100
fraction of solid on apparent wetted (f)	1/5

Maximum pressure, the pressure at the inlet due to the hydrostatic effects, is evaluated as 49 Pa. As a result, the maximum pressure that can be observed in the microchannel is lower than the critical pressure (P_c). Thus the water cannot penetrate the air cavities and the single phase assumption can be maintained. Within the scope of the study, the average velocity in the z-direction and temperature variation on the microchannels are investigated, numerically.

The results for the average velocity are organized in order to observe the fluid behaviour in terms of different depth and width values of the water domain in microchannel. For each value of the solid partition height (c), the plots of the average velocity in the z-direction ($\bar{V}_z$) versus for both the depth (d) and width (W) of the water are formed as shown in Figures 4.1 and 4.2, respectively. The simulations are examined for various regions and sections to interpret the effect of the parameters in Table 2.1, for temperature variation.

4.2 Marangoni phenomenon effect on the average velocity in the z-direction

Firstly, simulations were performed for various temperature differences (ΔT) and several water depth values (d) of 75, 150, 300 μm for a water width (W) of 400 μm. As presented in Figure 4.1, with an increase of water depth, the slope in the velocity behaviour decreases. The increase in the depth refers to the increase in the interface between air and water against proportional decrease in the effect of no-slip condition. It indicates that Marangoni effect is producing more driving force. On the other hand, the volume of the fluid is larger making the quantity of working fluid gain importance.

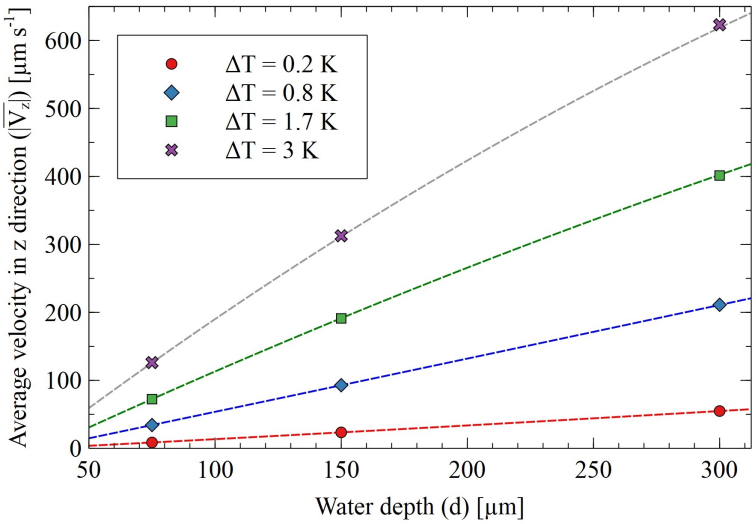
ΔT = 0.2 K
ΔT = 0.8 K
ΔT = 1.7 K
ΔT = 3 K
Average velocity in z direction ($\overline{|V_z|}$) [μm s^{-1}]
Water depth (d) [μm]
0
100
200
300
400
500
600
50
100
150
200
250
300

(i)

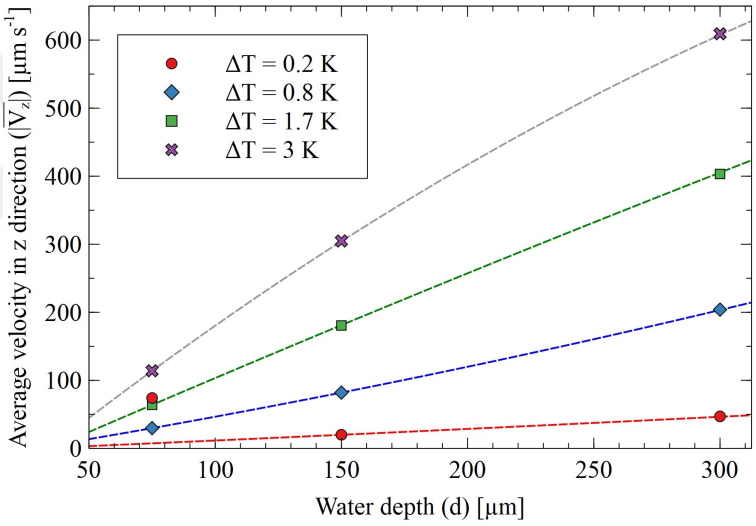
ΔT = 0.2 K
ΔT = 0.8 K
ΔT = 1.7 K
ΔT = 3 K
Average velocity in z direction ($\overline{|V_z|}$) [μm s^{-1}]
Water depth (d) [μm]
0
100
200
300
400
500
600
50
100
150
200
250
300

(ii)

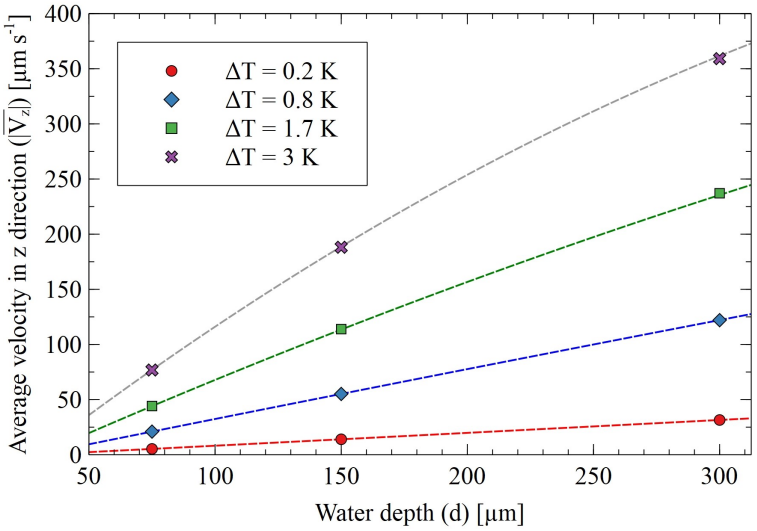

(iii)

Figure 4.1: Variation of average velocity ($\bar{V}_z$) by the water depth (d), with water width (W) of 400 μm and for the solid partition height (c) of (i) 25 μm, (ii) 50 μm, and (iii) 100 μm

Secondly, simulations were performed for various water widths of 400 μm, 800 μm, 2000 μm for the water depth of 75 μm with the results presented in Figure 4.2.

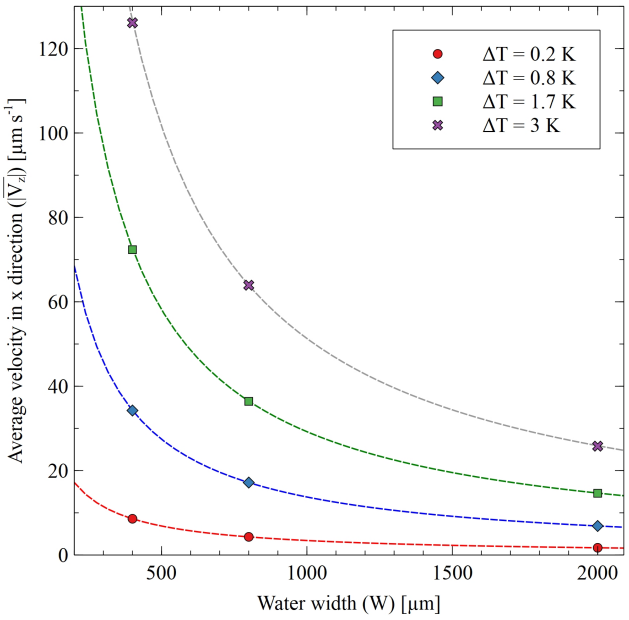

(i)

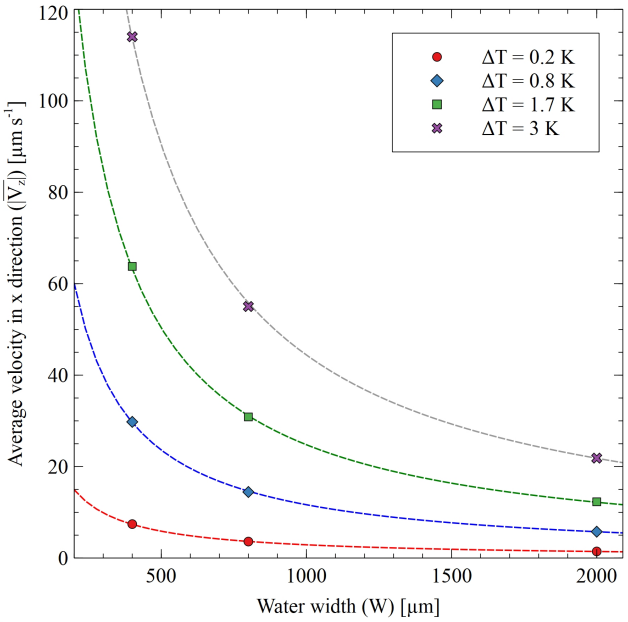

(ii)

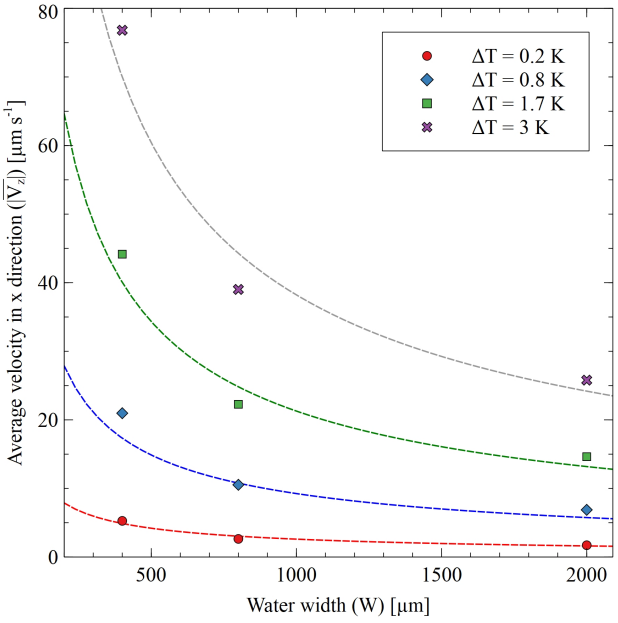

(iii)

Figure 4.2: Variation of average velocity ($\bar{V}_z$) by the water width (W), with water depth (d) of 75 μm and for the solid partition height (c) of (i) 25 μm, (ii) 50 μm, and (iii) 100 μm

The increase in the width (W) refers to the increase in the volume of the working fluid. It indicates that gravity forces begin to dominate the Marangoni effect that produces the driving force. In addition, the velocity magnitude created by the Marangoni effect should drive more fluid in the microchannel with greater width. As a result, the decrease in slope of the average velocity is observed in Figure 4.2.

4.3 Marangoni effect on temperature variations

To investigate temperature variation, nondimensional distance, $z^* = \frac{z}{L}$, through microchannel length and nondimensional temperature, $T^* = \frac{T-305}{\Delta T}$, are used.

4.3.1 Temperature variation in water domain

The temperature variation in the z-direction at the intersection line of midplanes of the microchannel is investigated. The flow in the microchannel is analyzed in terms of the impact of the solid partition height (c), the width (W) and depth (d) of the water. For the comparison, the simulations defined in Table 4.2 are selected as references. Figure 4.3 illustrates the temperature change in the center through the microchannel introduced for all cases in Table 4.2.

Table 4.2: The effects of temperature difference (ΔT) on temperature variation of water domain at $x = y = 0$ for Cases 1-4

Parameters	**Case 1**	**Case 2**	**Case 3**	**Case 4**
Solid partition height (c) [μm]	100	100	100	100
Water width (W) [μm]	400	400	400	400
Water depth (d) [μm]	150	150	150	150
Temp. difference (ΔT) [K]	0.2	0.8	1.7	3.0
Ma	0.45–0.64	0.68–3.50	1.34–12.13	-0.79–31.91

As ΔT is increased, the shear stresses on the water-air interfaces due to Marangoni effect get larger. The augmented shear stresses result in an increase of velocities in

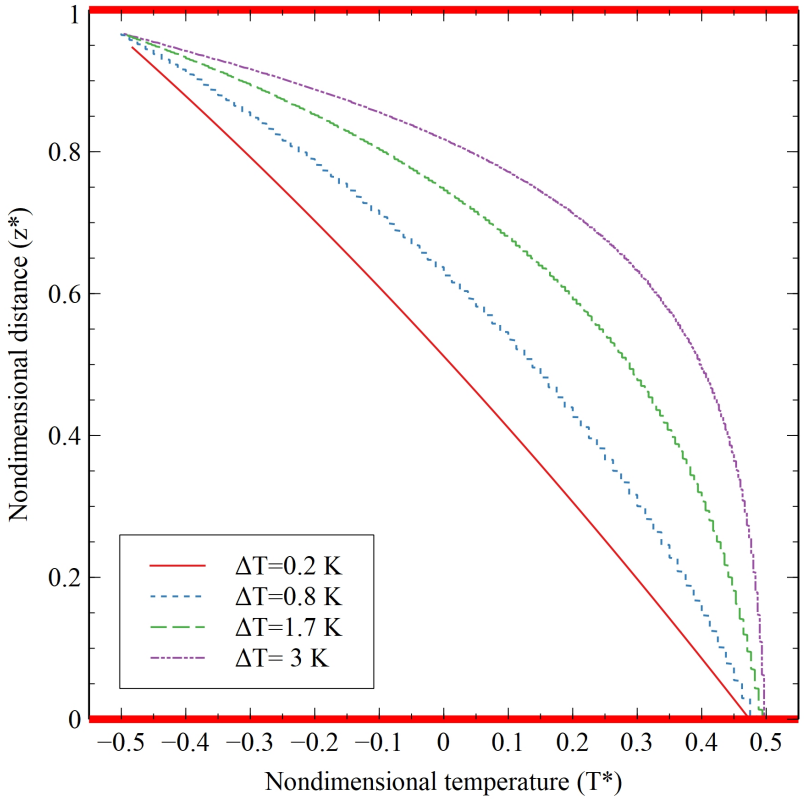

Figure 4.3: Temperature variation of water domain at $x = y = 0$ for Cases 1-4

the water domain which enhances the effects of convection thus the establishment of non-linear temperature variations as depicted in Figure 4.3. This behavior is resembled in the Ma values for each cavity.

Figure 4.4 depicts the z-direction temperature variations at the center through the microchannel defined in all cases in Table 4.3. This analysis aids to investigate the impact of the ratio of the solid partition height (c) to the air cavity height (a). With a decrease in the solid partition height (c), the total number of air cavities differs. Therefore, the total water-air surface area increases resulting in a magnification of Marangoni-induced shear stresses. These effects can be observed by comparing the Ma values given in Tables 4.2 and 4.3. Additionally, the non-linear temperature behaviors are observed in Figures 4.3 and 4.4 which is due to increase in shear stresses.

Table 4.3: The effects of temperature difference (ΔT) on temperature variation of water domain at $x = y = 0$ for Cases 5-8

Parameters	**Case 5**	**Case 6**	**Case 7**	**Case 8**
Solid partition height (c) [μm]	25	25	25	25
Water width (W) [μm]	400	400	400	400
Water depth (d) [μm]	150	150	150	150
Temp. difference (ΔT) [K]	0.2	0.8	1.7	3.0
Ma	0.38–0.71	0.05–4.28	0.17–16.92	-3.11–46.02

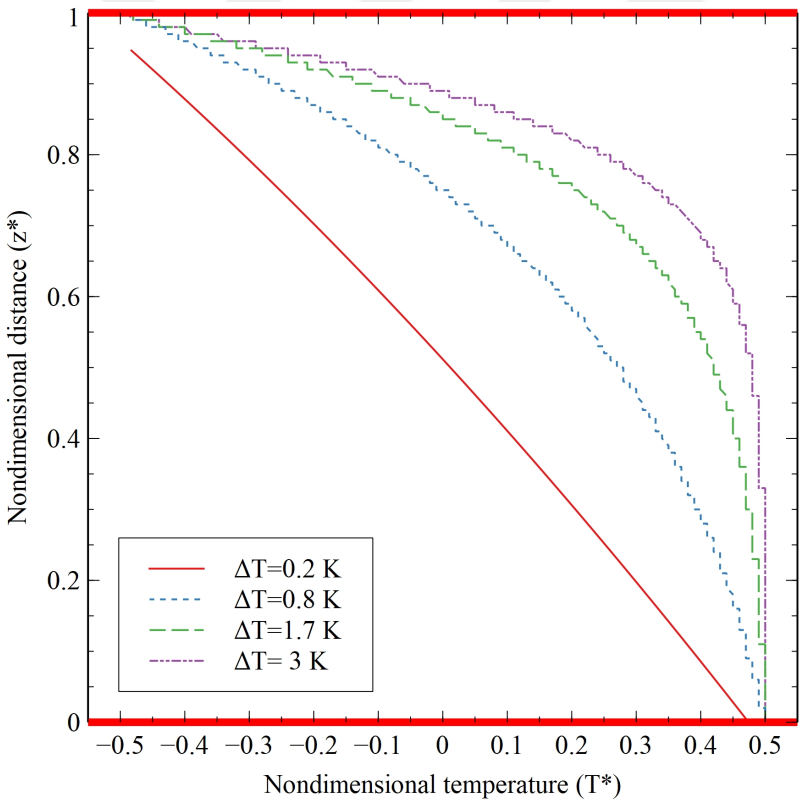

Figure 4.4: Temperature variation of water domain at $x = y = 0$ for Cases 5-8

Figure 4.5 demonstrates the z-direction temperature variation in the center through the microchannel defined in all cases in Table 4.4. This analysis leads to understanding the impact of the water depth (d).

Table 4.4: The effects of temperature difference (ΔT) on temperature variation of water domain at $x = y = 0$ for Cases 9-12

Parameters	**Case 9**	**Case 10**	**Case 11**	**Case 12**
Solid part. height (c) [μm]	25	25	25	25
Water width (W) [μm]	400	400	400	400
Water depth (d) [μm]	300	300	300	300
Temp. diff. (ΔT) [K]	0.2	0.8	1.7	3.0
Ma	0.12–0.94	-0.74–11.38	-0.21–37.77	-0.42–72.49

Greater water depth refers higher Marangoni effect in the microchannel due to the decrease in the effect of no-slip condition and the increase in the interface between air and water. Thus, the average velocity increases resulting in the non-linearity of temperature variation. In comparison with the results provided in Figure 4.4, the non-linear behavior is more pronounced in Figure 4.5. In line with this, the amount of deviation value for Ma is higher in all cases with the water depth of 300 μm in Table 4.4, compared to those in Table 4.3. Also the quantity of Ma are greater thereby surface tension gradients are more prominent than viscous forces.

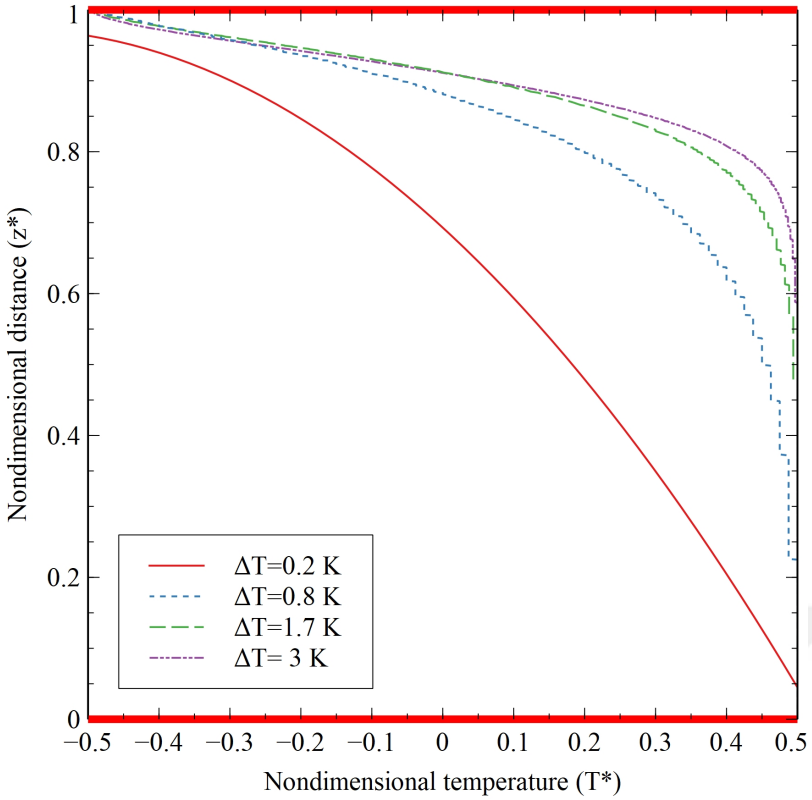

Figure 4.5: Temperature variation of water domain at $x = y = 0$ for Cases 9-12

Figure 4.6 gives information about the temperature variation in the center through the microchannel defined in all cases in Table 4.5. This analysis is for understanding the impact of the water width (W) in terms of the temperature difference.

Table 4.5: The effects of temperature difference (ΔT) on temperature variation of water domain at $x = y = 0$ for Cases 13-16

Parameters	**Case 13**	**Case 14**	**Case 15**	**Case 16**
Solid partition height (c) [μm]	25	25	25	25
Water width (W) [μm]	800	800	800	800
Water depth (d) [μm]	150	150	150	150
Temp. difference (ΔT) [K]	0.2	0.8	1.7	3.0
Ma	0.46–0.63	0.81–3.42	1.48–11.47	0.44–29.41

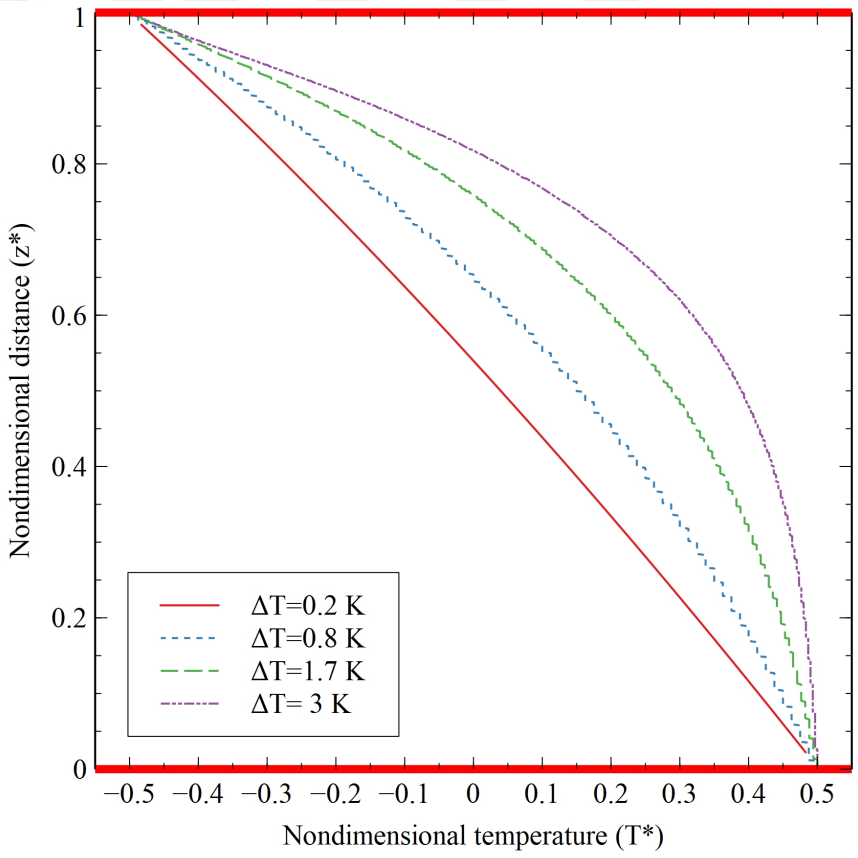

Figure 4.6: Temperature variation of water domain at $x = y = 0$ for Cases 13-16

Larger water width refers to higher volume of the fluid thus makes the gravity force important. The coefficients of the formula fitted to the temperature profile are demonstrated in Table 4.6. As a result, compared to Figure 4.3, the curves in Figure 4.6 are closer to the linear behaviour, since the terms causing non-linearity in the energy equation have relatively lower values. The result can be supported with a small difference in Ma of the cases in Table 4.5 than that of Table 4.2.

Table 4.6: The coefficients of the temperature profile in water domain with different water width (W)

The microchannel with solid partition height (c), water depth (d), and width (W), of 100 μm, 150 μm and 800 μm, respectively				
	ΔT=0.2 K	ΔT=0.8 K	ΔT=2.3 K	ΔT=3.0 K
A	305.1	305.39	305.86	306.5
B	-0.0399	-0.0563	-0.1066	-0.0273
C	-	-0.0199	0.0158	-0.0366
D	-	-	-0.0126	0.0126
E	-	-	-	-0.0059
The microchannel with solid partition height (c), water depth (d), and width (W), of 100 μm, 150 μm and 400 μm, respectively				
	ΔT=0.2 K	ΔT=0.8 K	ΔT=2.3 K	ΔT=3.0 K
A	305.11	305.39	305.87	306.48
B	-0.0397	-0.0466	-0.1196	0.0684
C	-	-0.0215	0.034	-0.1355
D	-	-	-0.0156	0.0553
E	-	-	-	-0.011
$T(z) = A + Bz + Cz^2 + Dz^3 + Ez^4$				

4.3.2 Temperature variations in solid domain

Temperature variations through the walls of microchannel are plotted for cases 1 through 16. Temperature boundary condition is applied only for the inlet and outlet in the water domain and in this section the temperature variation is given for the

vertical front and back walls. Accordingly, temperature behaviour in water domain determines the temperature variation through the solid domain. The temperature characteristics is obsevred in Figures 4.7 to 4.10 that illustrate the plots of nondimensional temperature variation (T^*) versus nondimensional distance (z^*). Temperature profiles through the z-direction in the solid domain are almost the same when compared to the temperature profiles through z-direction in the water domain. On the other hand, the temperature gradients in the x and y-directions are nearly zero.

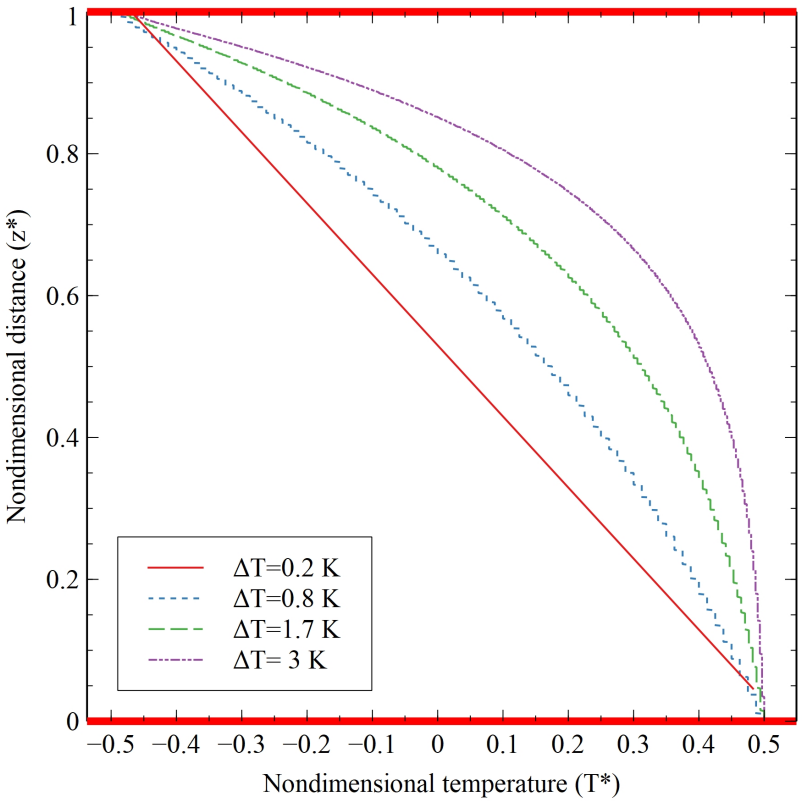

Figure 4.7: Temperature variation in the solid domain for Cases 1-4

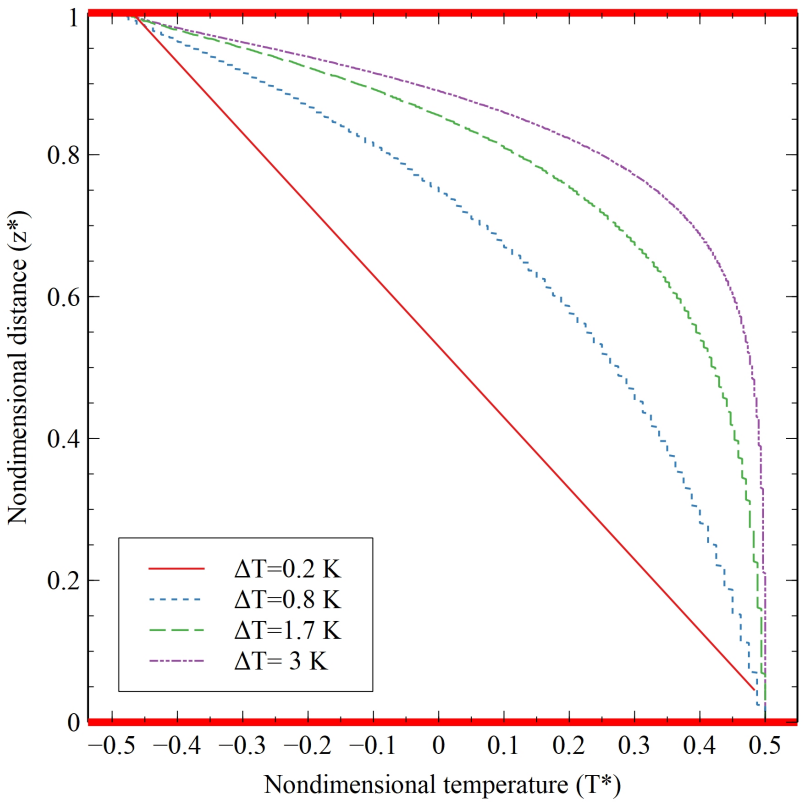

Figure 4.8: Temperature variation in the solid domain for Cases 5-8

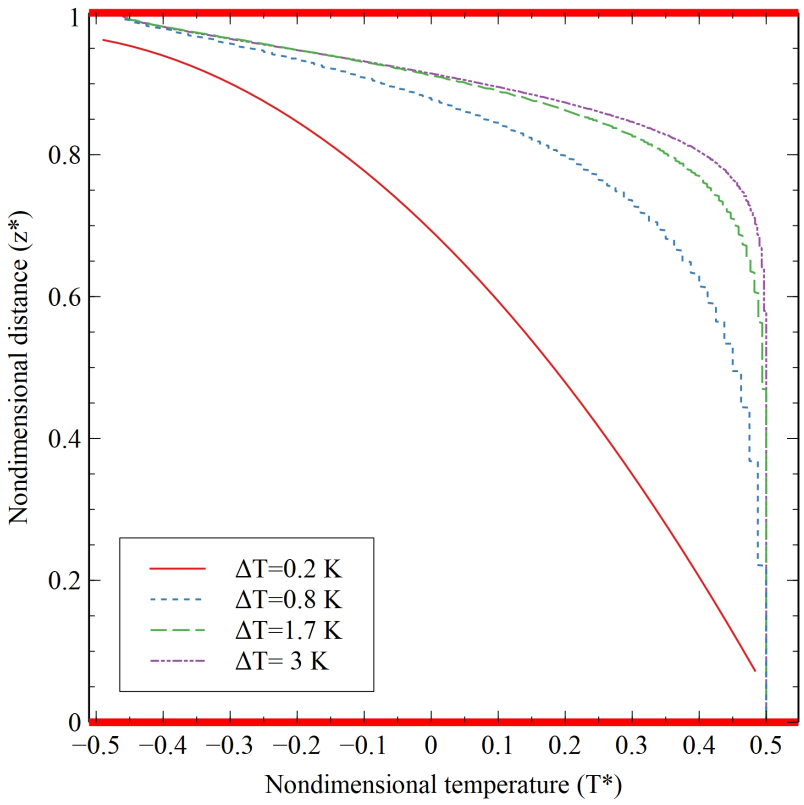

Figure 4.9: Temperature variation in the solid domain for Cases 9-12

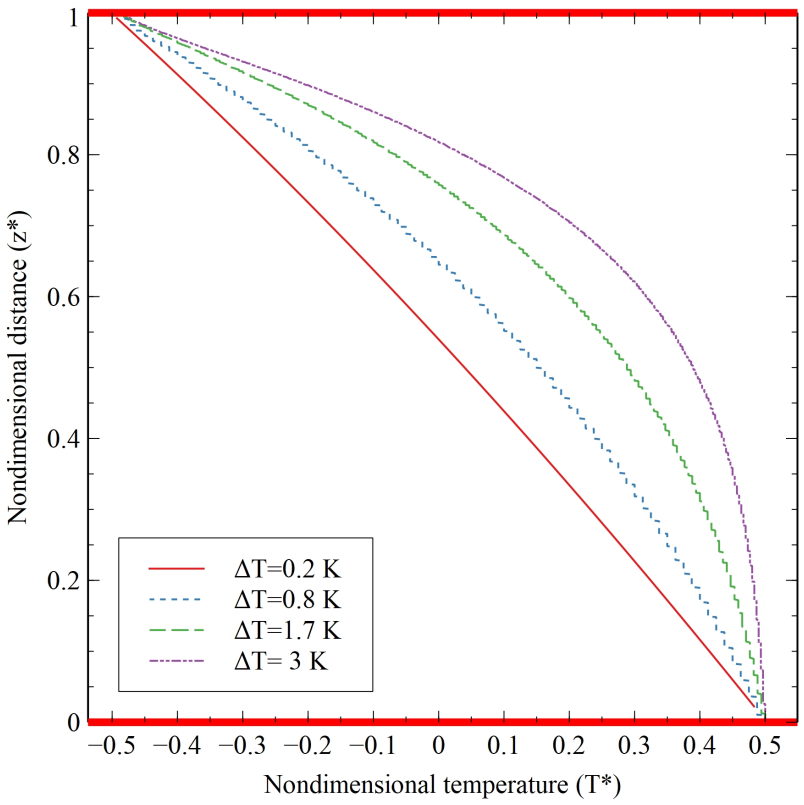

Figure 4.10: Temperature variation in the solid domain of for Cases 13-16

4.4 Marangoni effect on streamlines and velocity vectors in water domain

The temperature and velocity magnitudes are examined for three regions of the microchannel as presented in Figure 4.11. Each region is inquired based on the XZ and YZ plane in the middle of the microchannel.

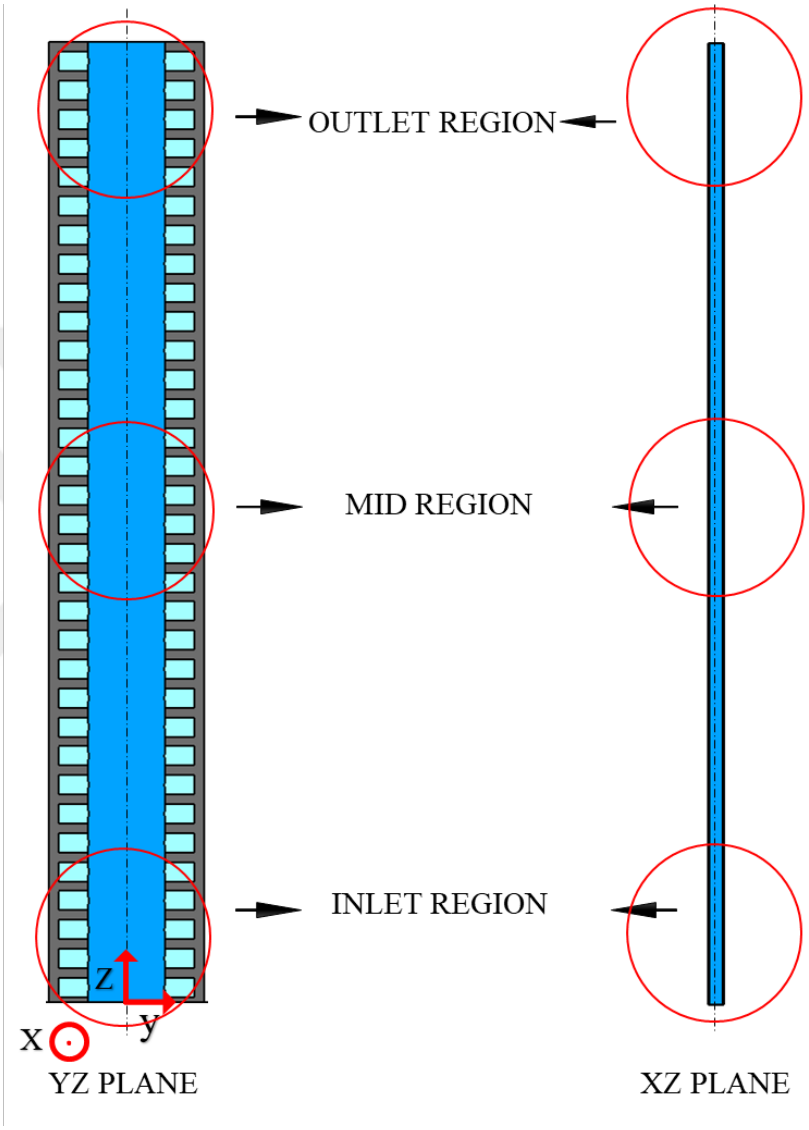

Figure 4.11: Focused regions on YZ plane (left) and XZ plane (right) to be examined in the microchannel

For all cases, there are some common results in terms of the velocity and temperature profiles. These similarities are explained via the reference cases in Figure 4.12. While XZ plane defined in Figure 4.11 of the microchannel can be observed in Figure 4.12i,

its YZ plane takes place in Figure 4.12ii. In addition, both velocity magnitude (on the left) and temperature variation (on the right) are demonstrated in the same image thanks to the symmetric behaviour of the flow.

Marangoni effect, the driving force of the microchannel, is directly related to the temperature change that is the essential component of the surface tension. This relation can be noted via Ma increasing with temperature differences in Table 4.3. The outlet region of the microchannel has the greatest temperature gradient as given in Figure 4.4 as well velocity magnitude in Figure 4.12ii in all regions.

Another common inference is related to the maximum and zero values of the velocity in the microchannels. Due to slip condition in Marangoni boundary, the maximum velocity magnitude is observed in the side of this boundary, whereas, the inner wall of the microchannel has zero velocity magnitude because of no slip condition.

Furthermore, the direction of the velocity vectors have similar characteristics. YZ plane in the mid region of the microchannel illustrates both straight and reverse velocity vectors. This obscure behaviour is resulted from the equation of mass conversation. There are two opposite forces in the microchannel. Marangoni boundary has provided an effect to the system like Coutte flow. On the other hand, the system has an inclination to conserve its shape owing to having incompressible behaviour.

As for XZ plane, although the direction of the vectors is in reverse direction in the outlet region, it is in the direction of flow in the inlet region. The temperature gradient as the driving force resulted from Marangoni effect is relatively more in the outlet region. Therefore, more reversed flow is expected in this region due to the equation of mass conversation.

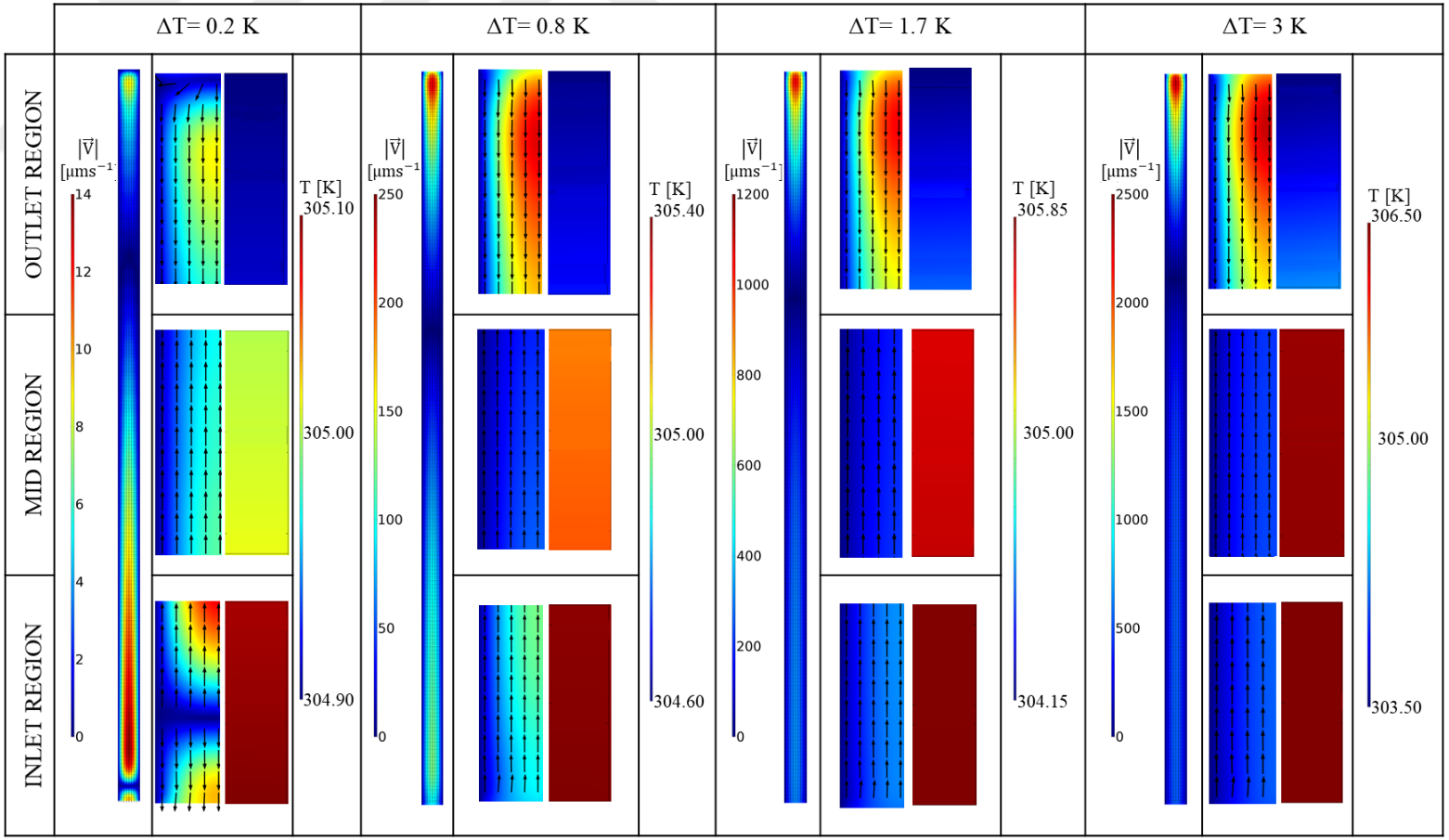

(i) Velocity magnitude and vectors (left) and temperature (right) on XZ plane

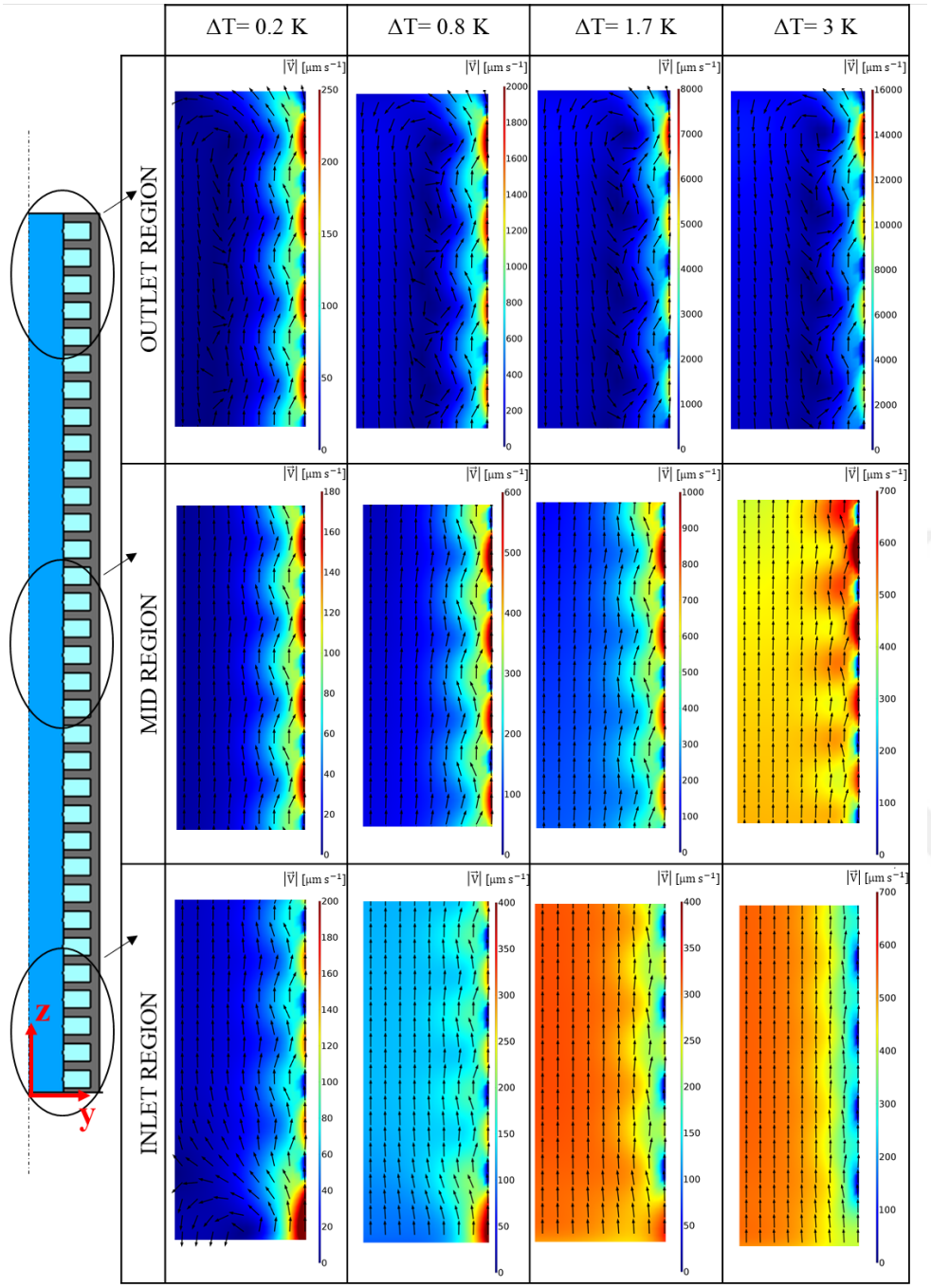

(ii) Velocity magnitude and vectors on YZ plane

Figure 4.12: Velocity vectors on (i) XZ and (ii) YZ planes of the mid of the microchannel with solid partition height (c), depth (d), and width (W), of 25 μm, 150 μm and 400 μm, respectively

4.4.1 The effects of the solid partition height

The results for the microchannels having different solid partition height (c) are used, with the same water depth and width values, 150 μm and 400 μm, respectively. Figure 4.12 depicts the vectors on the surface referring to velocity magnitude for the microchannel with solid partition height (c) of 25 μm and Figure 4.13 gives the same information for the microchannel with solid partition height (c) of 100 μm. Marangoni boundary takes place with the ratio of 80% in the microchannel with solid partition height (c) of 25 μm, however, the ratio is 50% in the microchannel with solid partition height (c) of 100 μm. Since the microchannel with solid partition height (c) of 25 μm provides larger water-air interface, its velocity magnitude is greater. Also Ma illustrating the importance of Marangoni effect in the microchannel can be utilized to explain the results. The microchannel with solid partition height (c) of 100 μm has Ma between -0.79 – 31.91 as given in Table 4.2 while the microchannel with solid partition height (c) of 25 μm has Ma between -3.11 – 46.02 in Table 4.3. As expected, it is inferred that surface tension forces are more dominant in the microchannel having more area for Marangoni boundary.

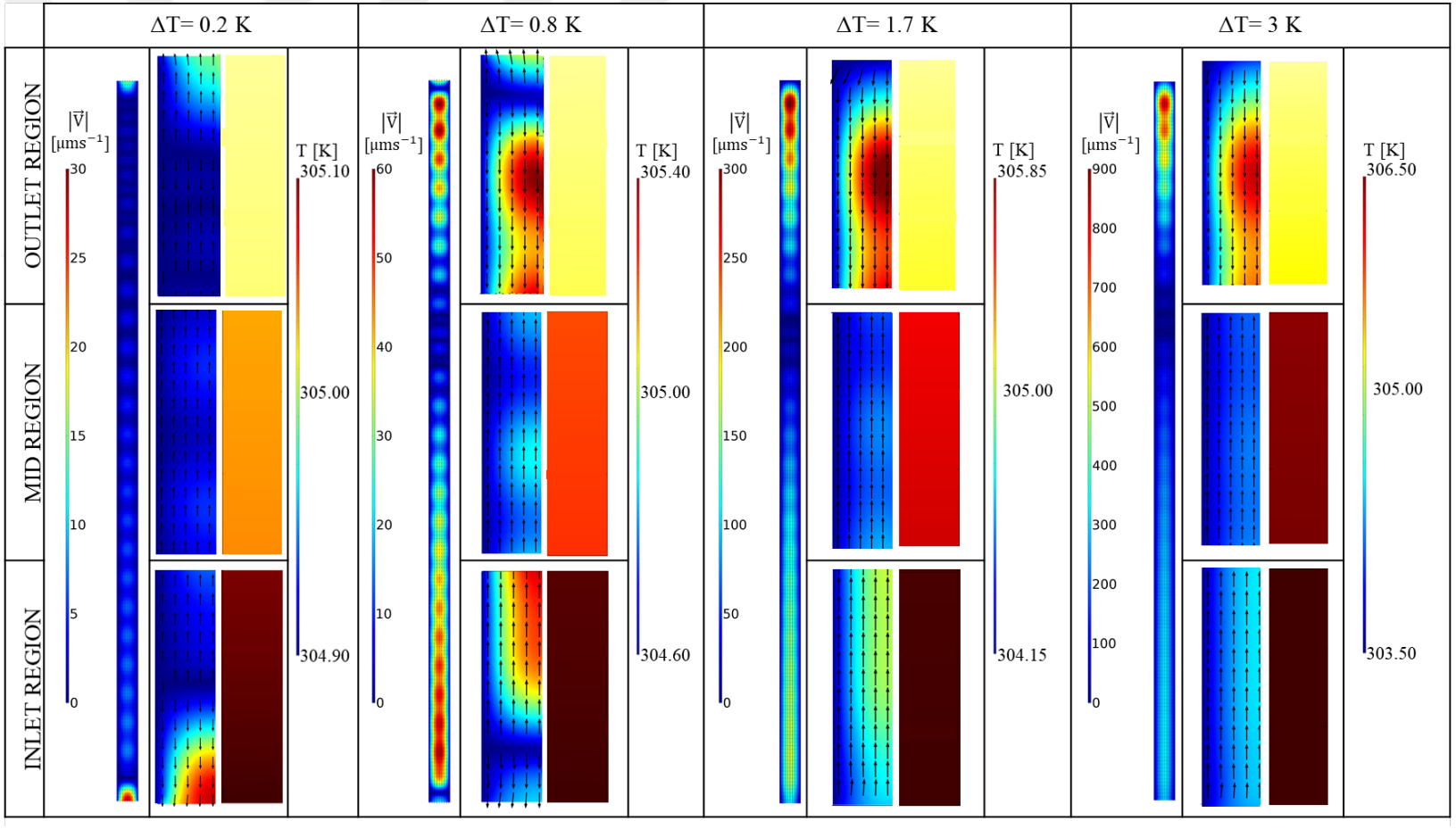

(i) Velocity magnitude and vectors (left) and temperature (right) on XZ plane

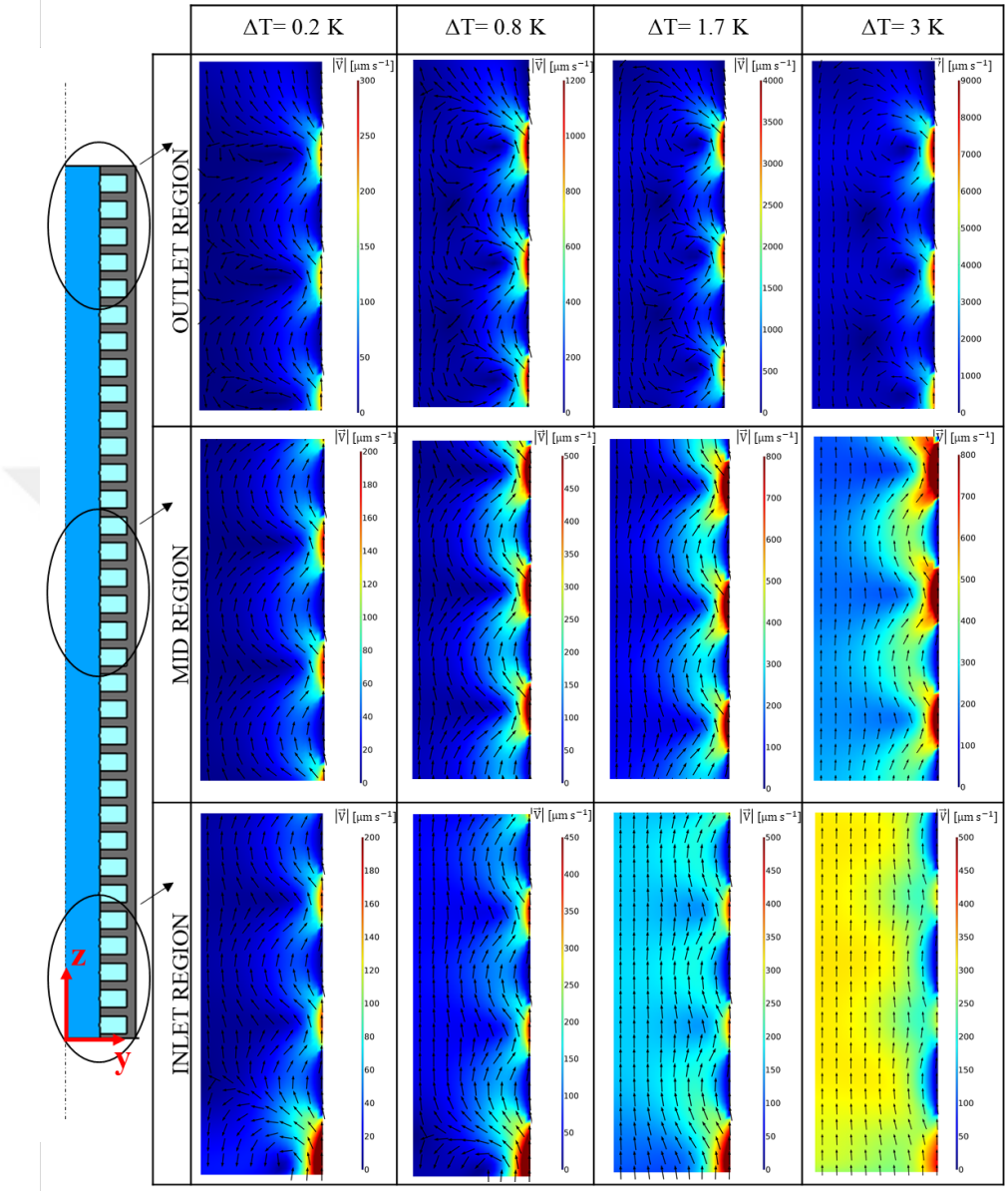

(ii) Velocity magnitude and vectors on YZ plane

Figure 4.13: Velocity vectors on (i) XZ and (ii) YZ planes of the mid of the microchannel with solid partition height (c), depth (d), and width (W), of 100 μm, 150 μm, and 400 μm, respectively

4.4.2 The effects of the water depth

The results for the water depth values of 150 μm and 300 μm are used, the same solid partition height (c) and width (W) values, 25 μm and 400 μm, respectively. When Figure 4.12 depicts the velocity vectors on the surface referring to temperature variation for the microchannel with water depth of 150 μm, Figure 4.14 gives the same information for the microchannel with water depth of 300 μm.

Because of negligible temperature change through the depth of the microchannel, forces induced by Marangoni effect are not affected directly in an interface. However, the microchannel in Figure 4.14 has relatively less effect of zero velocity vector resulted from no-slip condition on the walls of the microchannel. Also an increase in water depth results in temperature variation with more temperature gradient as mentioned in Section 4.3.1. Thus its velocity magnitude as well as Ma are much larger, compared to the microchannel in Figure 4.12.

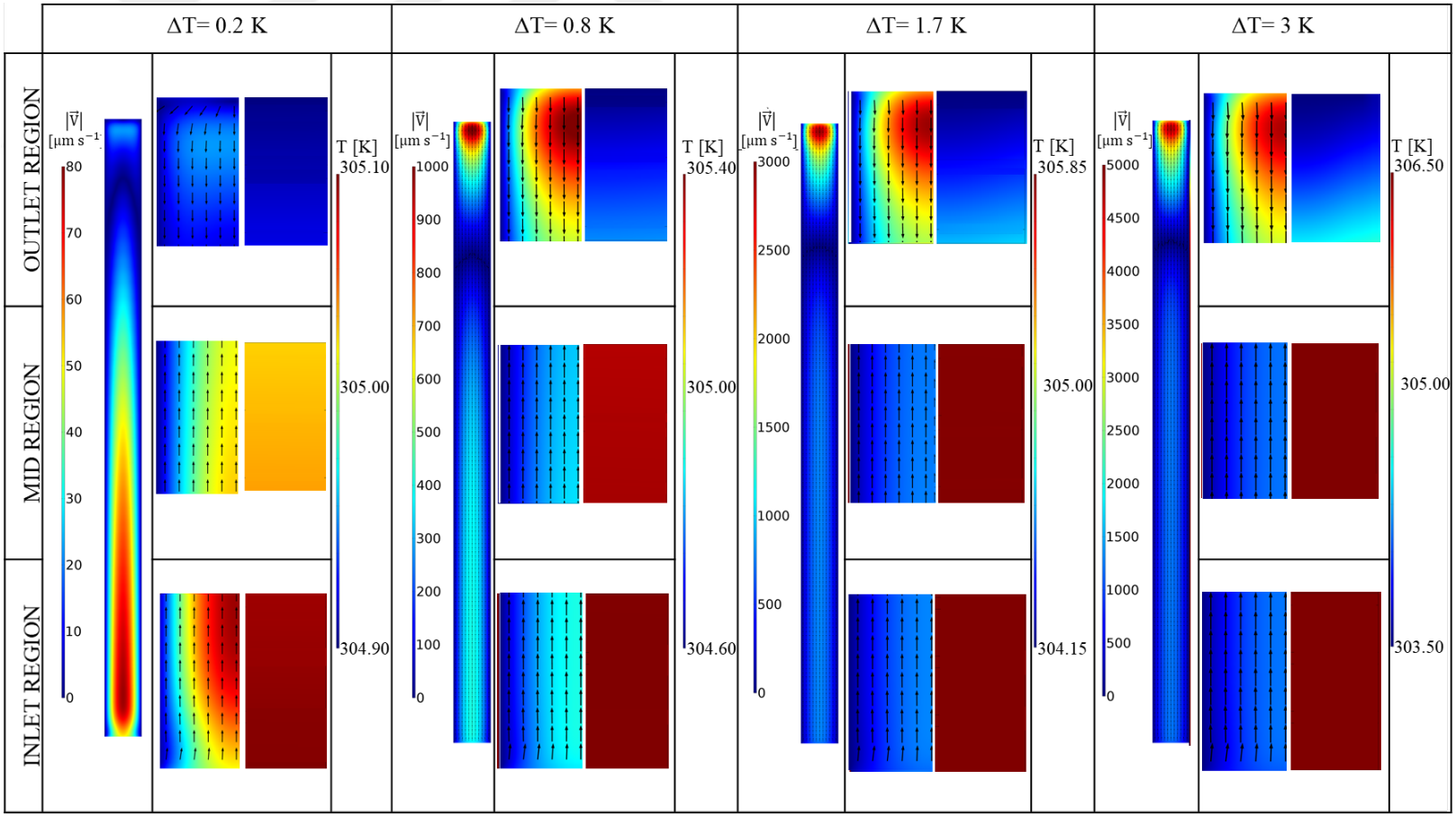

(i) Velocity magnitude and vectors (left) and temperature (right) on XZ plane

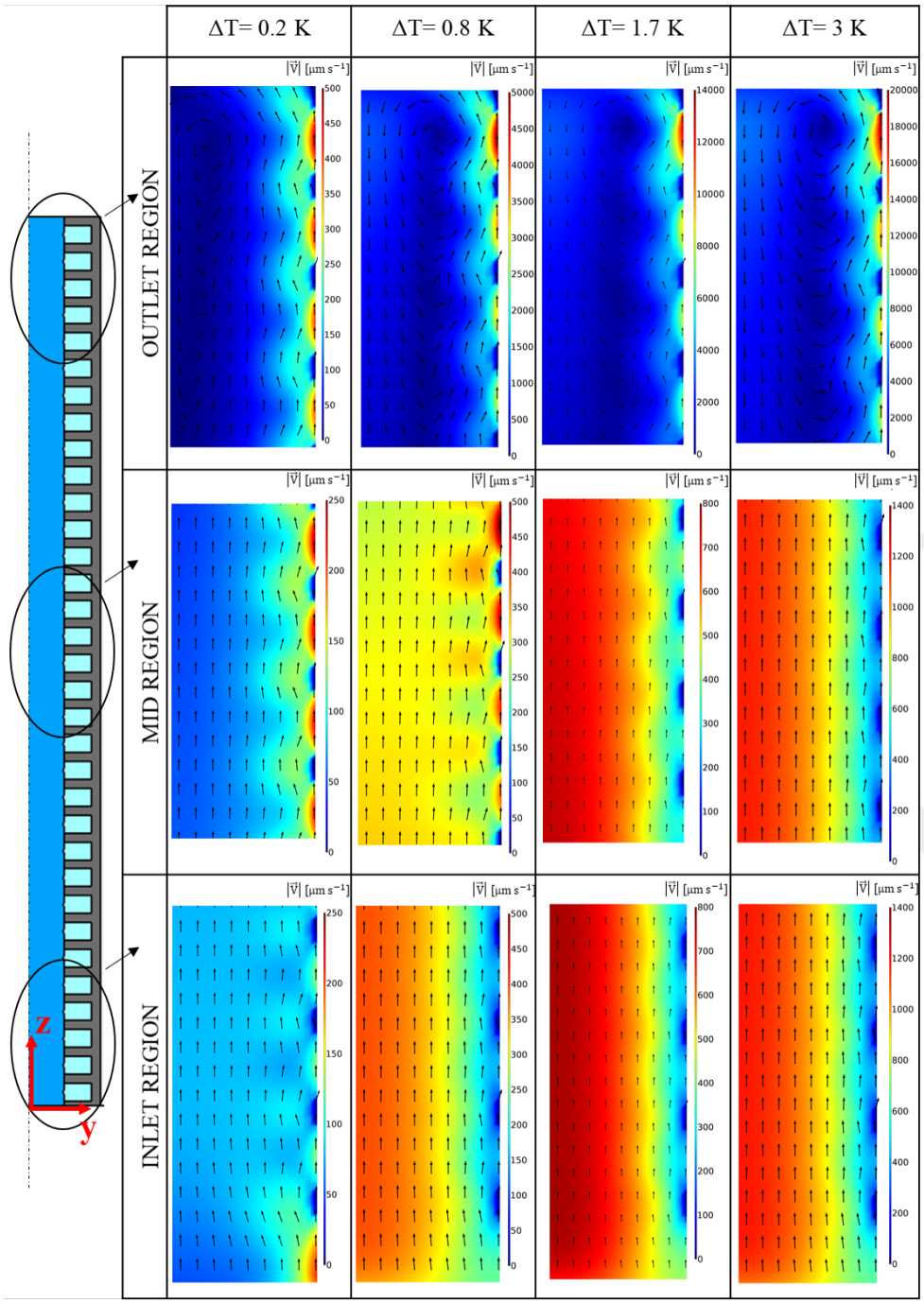

(ii) Velocity magnitude and vectors on YZ plane

Figure 4.14: Velocity vectors on (i) XZ and (ii) YZ planes of the mid of the microchannel with solid partition height (c), depth (d), and width (W), of 25 μm, 300 μm and, 400 μm, respectively

4.4.3 The effects of the water width

To compare the microchannels, the results for the width values of 400 μm and 800 μm are used, with the solid partition height (c) and depth (d) values, 25 μm and 150 μm, respectively. Figure 3.11 depicts the velocity vectors on the surface referring to velocity magnitude for the microchannel with width of 400 μm and Figure 4.15 gives the same behaviour for the microchannel with width of 800 μm.

The microchannel shown in Figure 4.15 has more volume of water than that in Figure 4.12 although it has the same size of interface between air and water. Since the water width (W) is doubled, the velocity magnitude created by interfacial forces is decreased. On the other hand, the wavy-type motion near the Marangoni boundary due to the balance between the body forces and Marangoni stresses is depicted in both Figures. This fluid behavior covers the most of microchannel in Figure 4.12, whereas, ends almost in the one third of the microchannel in Figure 4.15 because of the microchannel sizes.

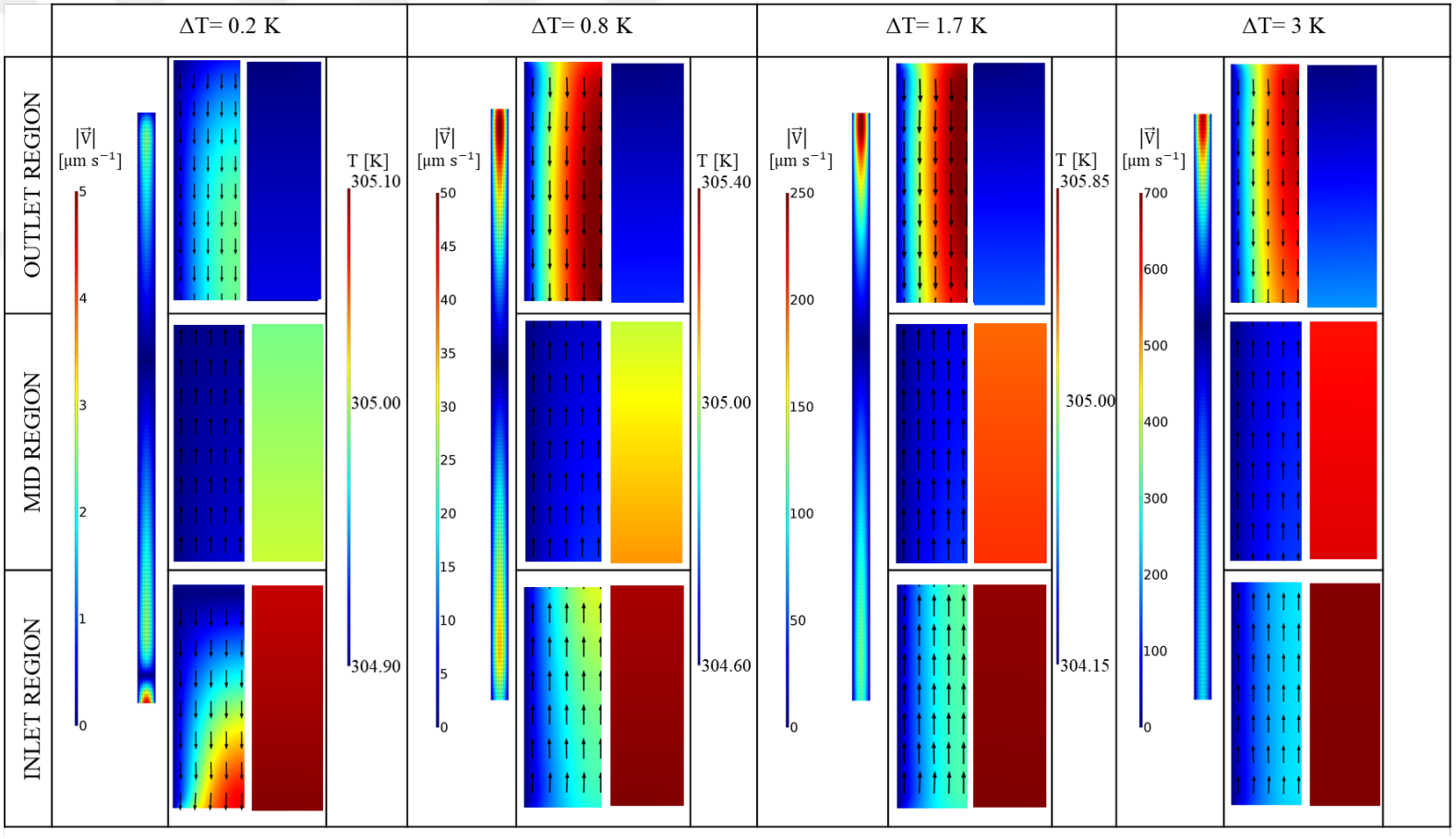

(i) Velocity magnitude and vectors (left) and temperature (right) on XZ plane

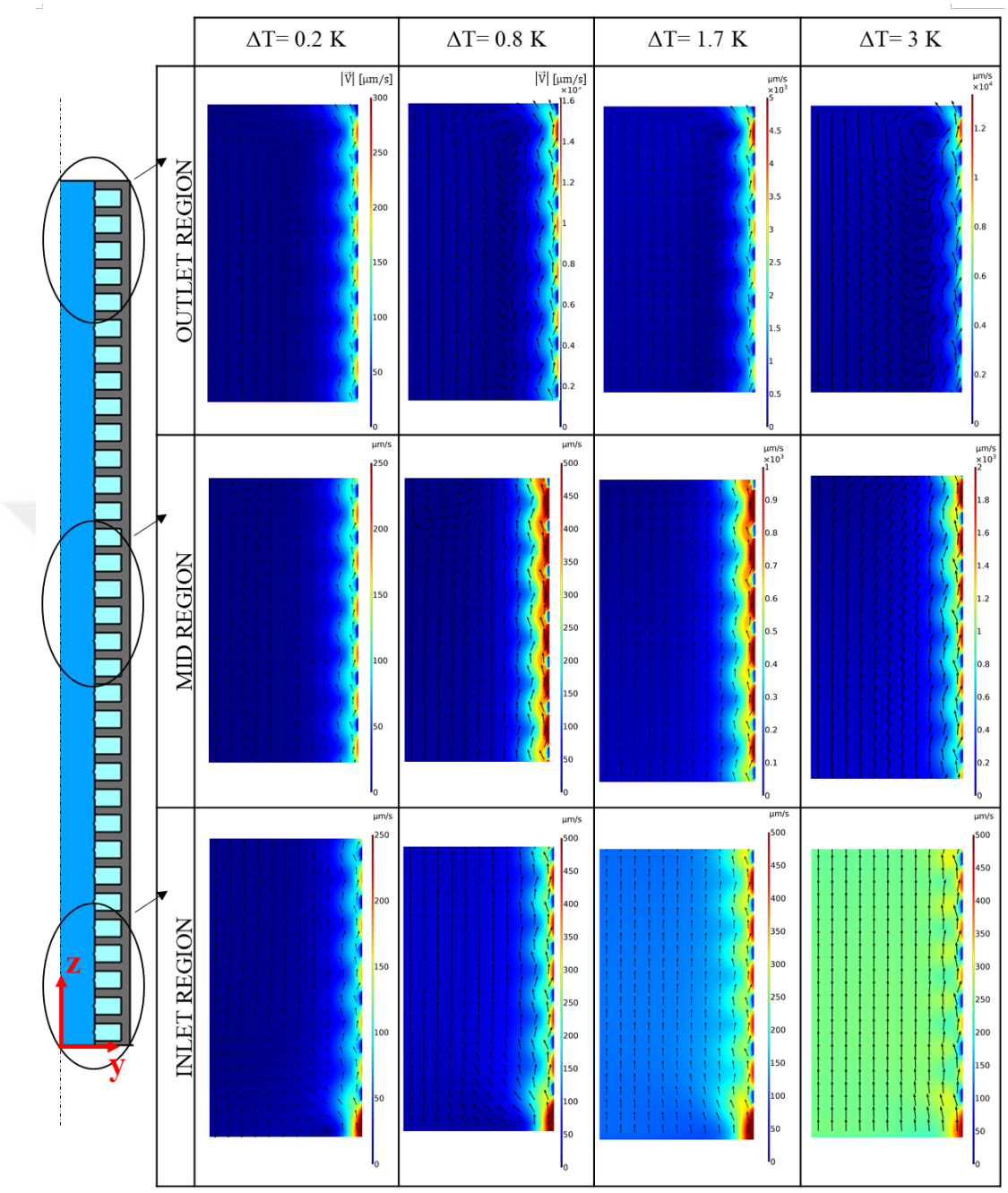

(ii) Velocity magnitude and vectors on YZ plane

Figure 4.15: Velocity vectors on (i) XZ and (ii) YZ planes of the mid of the microchannel with solid partition height (c), depth (d), and width (W), of 25 μm, 150 μm, and 800 μm, respectively

4.4.4 Flow characterization

As presented in Figure 4.12-4.15, the direction of flow changes in a specific region through the microchannel. The important regions that show the direction change of flow are depicted in Figures 4.16 to Figure 4.19. To analyse the flow characterization in detail, the particular region between 2700 μm < z < 4000 μm is focused. A strong relation between the temperature gradient and the location of direction change is observed.

A linear distribution is observed in water domain with temperature difference (ΔT) of 0.2 K. Therefore, the position in which the direction of vectors changes does not depend on temperature gradient, directly but gravity and Marangoni effect. Gravity leads only to a motion in z-direction, whereas Marangoni effect creates motion in both the z and x-directions due to interfacial interactions. This causes a complex behaviour in the flow. The reverse flow is observed in different locations in the z-direction which is due to the magnitude of Marangoni effect and the assumptions and limitations of the current numerical model.

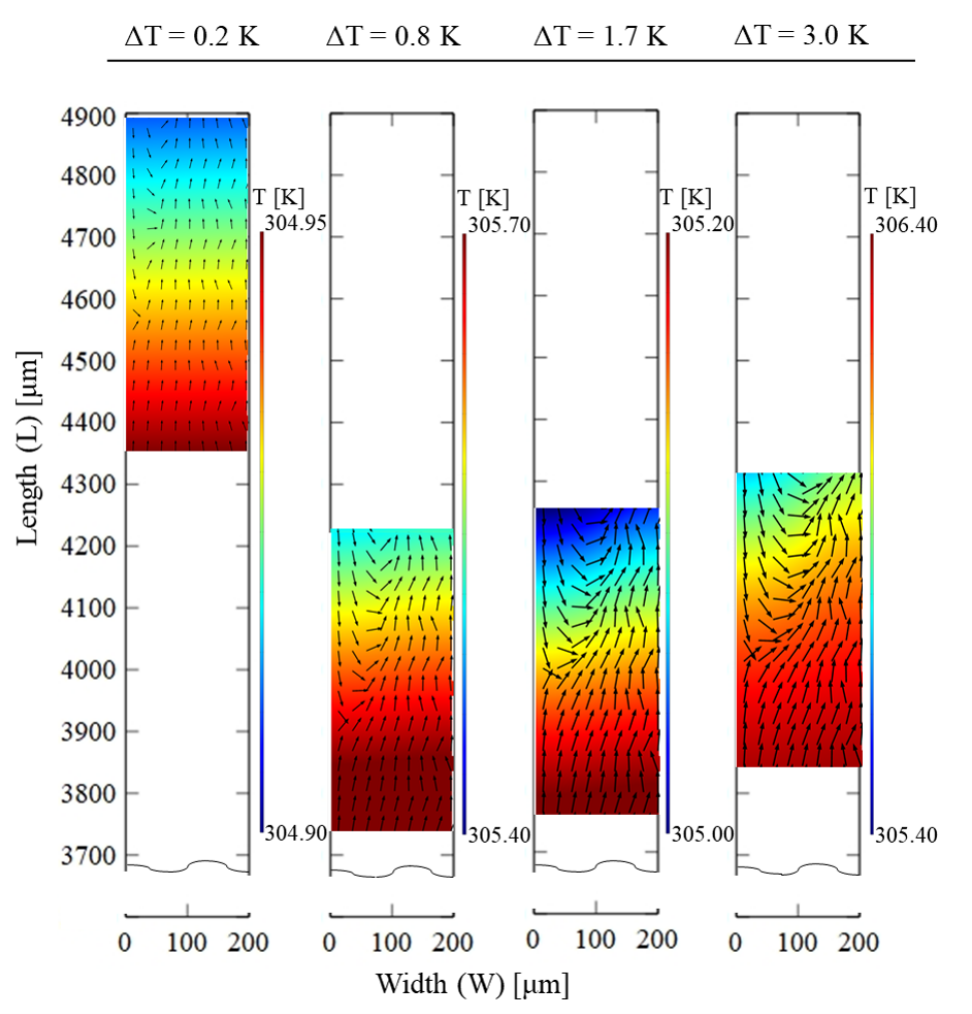

Figure 4.16: Flow characterization in the water domain with solid partition height (c), depth (d), and width (W), of 25 μm, 300 μm and 400 μm, respectively

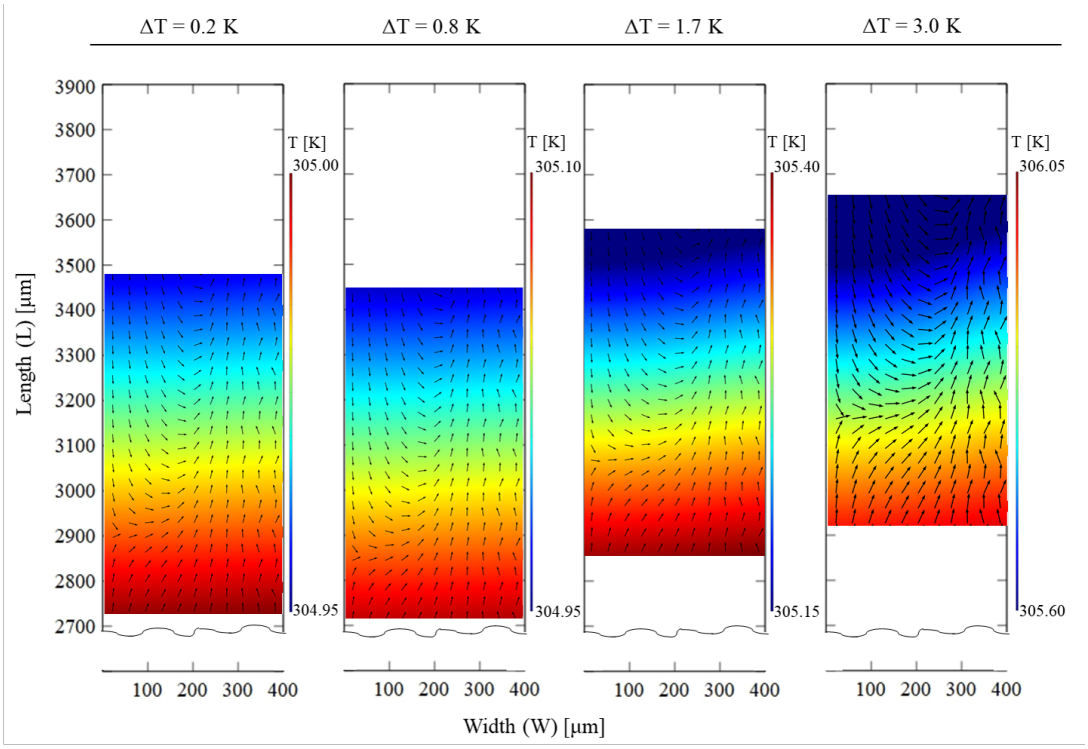

Figure 4.17: Flow characterization in the water domain with solid partition height (c), depth (d), and width (W), of 25 μm, 150 μm, and 800 μm, respectively

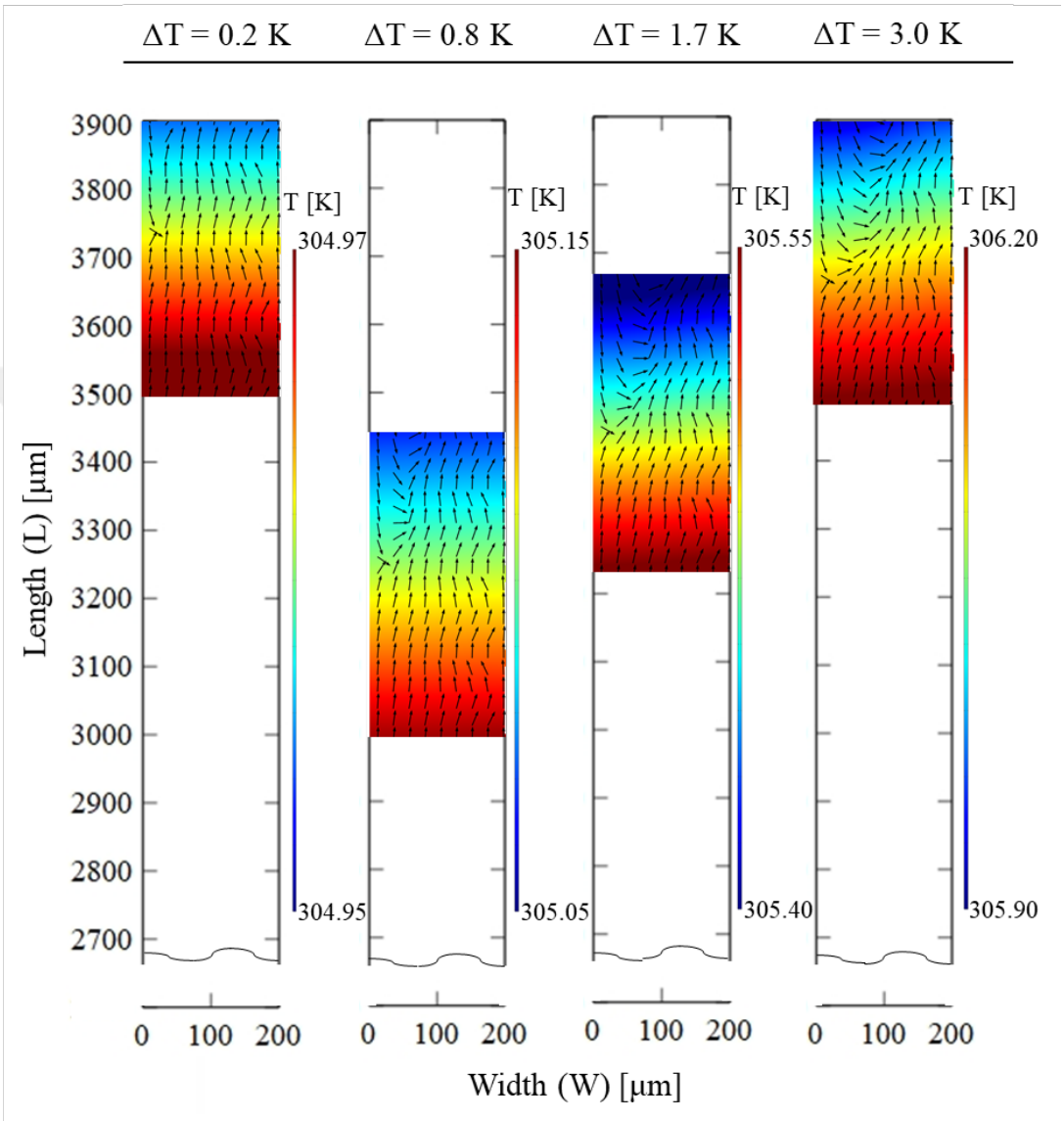

Figure 4.18: Flow characterization in the water domain with solid partition height (c), depth (d), and width (W), of 25 μm, 150 μm and 400 μm, respectively

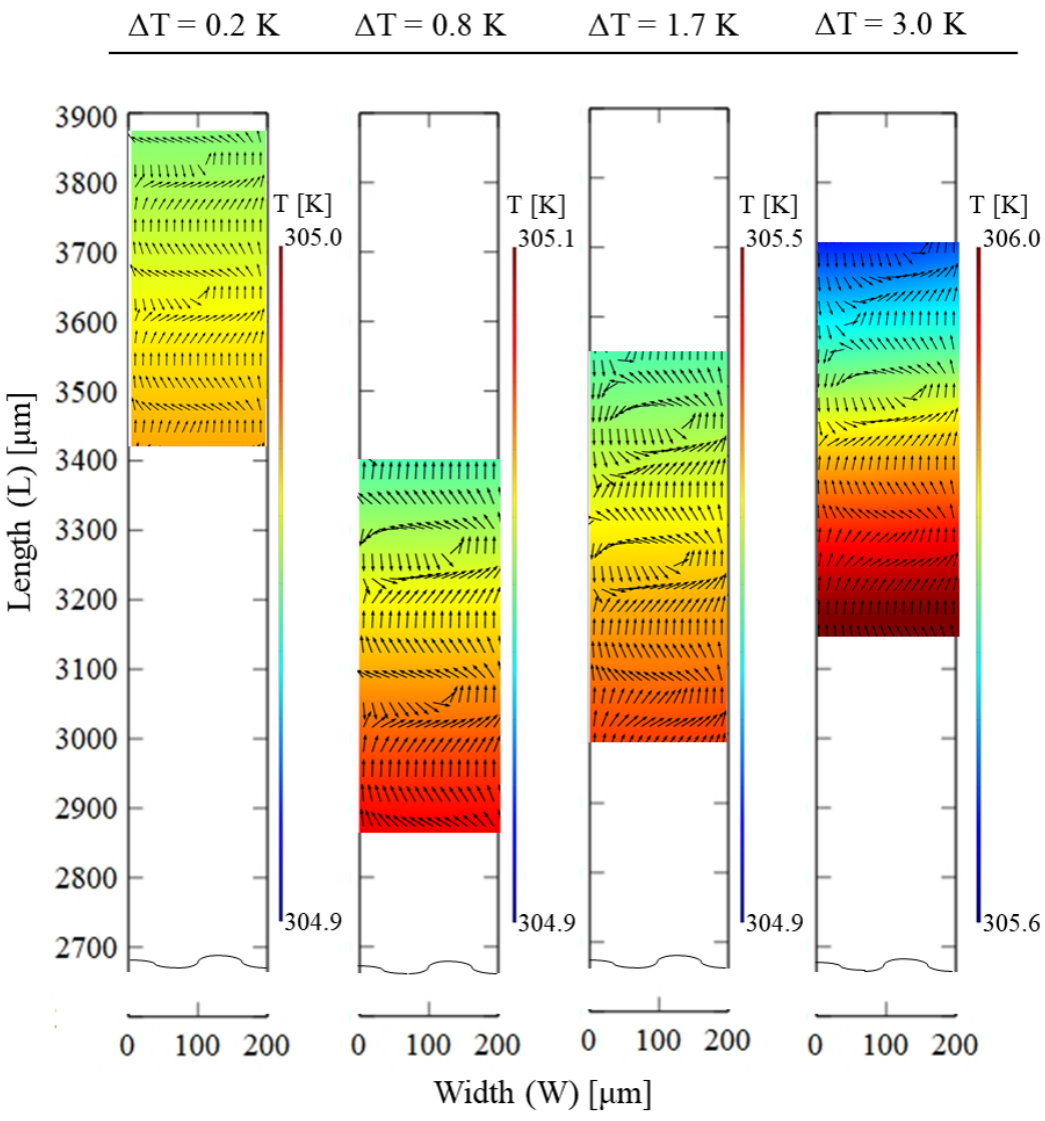

Figure 4.19: Flow characterization in the water domain with solid partition height (c), depth (d), and width (W), of 100 μm, 150 μm, and 400 μm, respectively

For the nonlinear temperature variation in the other microchannels, absolute maximum temperature gradient is used as a measurement method. Increase in temperature difference (ΔT) results an increase in the non-linearity as well as absolute maximum temperature gradient as aforementioned in Section 4.3.1. Also the Marangoni effect rises due to the growth in temperature difference as understood via the boundary definition in Eqn. 2.4. Not only the quantity but also deviation of Ma are higher in those cases. As a result, when temperature difference (ΔT) increases, the distance where the the vector's direction changes is closer to the outlet as depicted in Figure 4.16-4.19.

Like the effect of temperature difference (ΔT), the change of vector's direction is observed closer to the outlet exposing higher Marangoni effect in terms of other factors. The values of higher water depth (d), lower solid partition height (c) and water width (W) refer to higher Marangoni effect as aforementioned in Section 4.4.2, 4.4.1, and Section 4.4.3, respectively. Corresponding factors lead to higher temperature gradient. Thus the expectation is that distance where the vector's direction changes is longer. In comparison with the microchannels in Figure 4.18, the change in vectors' direction is closer to the outlet in all microchannels with higher depth (d) in Figure 4.16. Compared to the microchannels in Figure 4.19, the distance where the direction of vector changes is longer in the all microchannels with lower solid partition height (c) in Figure 4.18. As last comparison, the direction of vectors in the water domains with lower width (W) in Figure 4.18 changes closer to the outlet than those in the microchannels in Figure 4.17.

CHAPTER 5

CONCLUSION AND FUTURE WORK

The current work aims to investigate the Marangoni-induced flow in the vertical microchannels. Average velocity, temperature gradient and the structure of flow are elaborated for various sizes of the microchannels. Numerical study is constructed by COMSOL Multiphysics 5.6.

First, the horizontal version of the related system is validated by the study of Amador et al. [35]. The fitted results are obtained for the various sizes of the microchannel and several working fluids. Then targeted vertical microchannel is focused on. Because the microchannel height, the pressure in inlet increases in the transition horizontal to vertical, Cassie-Baxter condition is controlled which illustrates the fluid behavior in the hydrophobic system having air cavities. The vertical microchannel in the thesis is made of polydimethylsiloxane (PDMS) having hydrophobic characteristic. As a result of satisfying Cassie-Baxter condition, it is ensured that air cavities in the vertical system do not fill with water. Thus single phase assumption is maintained.

The simulation is constructed by various sizes of the single solid partition height (c) contacting with the water, water width (W) and depth (d). After that, their influence on temperature distribution, velocity magnitude and the structure of the fluid flow are interpreted. Marangoni numbers calculated for each cell proves the expectation and outputs.

As a result of the simulations, the relation between outputs and relation between parameter and output are considered separately. A rise in the width (W) results in more effective gravity forces while a growth in the height of solid partition (c) contacting with the water means less proportional Marangoni boundary. Both lead to decline in the effect of Marangoni forces. Thus average velocity as well absolute maximum temperature gradient decrease due to energy equation solved in coupled way. In the

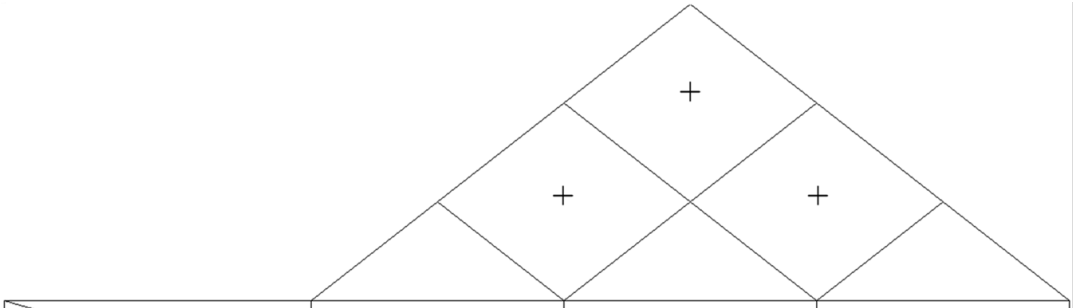

Parameters \ Output	Average velocity magnitude in water	Absolute maximum temp. gradient	Distance where vector directions change
Water width (W)	−	−	−
Water depth (d)	+	+	+
Solid partition height (c)	−	−	−

Figure 5.1: The relation between parameters and output

line with this, distance where the the direction of vector changes from the origin decreases since temperature as well flow structure changes drastically closer to the outlet with the increase in temperature gradient. As for a rise in depth (d), no-slip condition effect decreases proportionally and Marangoni forces are more prominent. Thus all outputs aforementioned increase. Furthermore, various temperature differences (ΔT) between inlet and outlet are applied in order to construct the simulations. As temperature difference (ΔT) increases in the simulations, velocity magnitudes and absolute maximum temperature gradients grow. It is expected because of the relation of velocity and temperature in energy equation. Inverse or direct proportion of the outputs and parameters are given in Table 5.1 briefly.

An investigation for the effect of surface tension in microfluidics provides a useful resource for the researches in bio-science as well cooling systems in microelectronics. Marangoni forces are the intrinsic forces that can be obtained without any pumping power requiring cost. Moreover, providing slip condition to the system leads to decrease in pressure drop. To concentrate this topic in microfluidics contributes not only analysis into bio-science but also innovation in terms of cost reduction and less pressure drop in microfluidics. As a future work, the study can be set up for unsteady condition. Thus when the rotational movement begins is found. Especially it can give a useful analysis in the microsystems with flexible material, namely vines

in which an expansion results in some adverse effects on the body. Another work can be related with flow control. In nanofluidics, the augmentation of nanoparticles in the microfluidics is an important concern because of huge pressure drop. There are some methods for mixing to prevent from accumulation of them. The rotational movement in Marangoni convection can be a different approach for this area. Last, due to requiring Cassie-Baxter state analysis mentioned in Section 2.1, the effect of the cavity height (a) is not inquired in the thesis. Investigating different sizes of the cavity height (a), cooling in the cavity of the printed circuit boards (PCB) can be discussed in terms of the micro devices with different sizes.

REFERENCES

[1] G. M. Whitesides, "The origins and the future of microfluidics," *Nature*, vol. 442, no. 7101, p. 368–373, 2006.

[2] R. Vitorino, S. Guedes, J. P. da Costa, and V. Kašička, "Microfluidics for peptidomics, proteomics, and cell analysis," *Nanomaterials*, vol. 11, no. 5, p. 1118, 2021.

[3] N. Convery and N. Gadegaard, "30 years of microfluidics," *Micro and Nano Engineering*, vol. 2, p. 76–91, 2019.

[4] D. Khorsandi, M. Nodehi, T. Waqar, M. Shabani, B. Kamare, E. N. Zare, S. Ersoy, M. Annabestani, M. F. Çelebi, and A. Kafadenk, "Manufacturing of microfluidic sensors utilizing 3D printing technologies: A production system," *Journal of Nanomaterials*, vol. 2021, p. 1–16, 2021.

[5] B. E. Rapp, *Microfluidics: Modeling, mechanics and mathematics*. Elsevier, 2022.

[6] F. Peters and D. Arabali, "Interfacial tension between oil and water measured with a modified contour method," *Colloids and Surfaces A: Physicochemical and Engineering Aspects*, vol. 426, p. 1–5, 2013.

[7] N. B. Vargaftik, B. N. Volkov, and L. D. Voljak, "International tables of the surface tension of water," *Journal of Physical and Chemical Reference Data*, vol. 12, no. 3, p. 817–820, 1983.

[8] D. Villers and J. K. Platten, "Temperature dependence of the interfacial tension between water and long-chain alcohols," *The Journal of Physical Chemistry*, vol. 92, no. 14, p. 4023–4024, 1988.

[9] M. Masoudi, M. Khosravi, B. Rostami, and P. Abolhosseini, "Effect of Bénard-Marangoni flow on the bypassed oil recovery: Micromodel study," *Journal of Petroleum Science and Engineering*, vol. 178, p. 1067–1078, 2019.

[10] A. D'Aubeterre, R. Da Silva, and M. Aguilera, "Experimental study on

Marangoni effect induced by heat and mass transfer," *International Communications in Heat and Mass Transfer*, vol. 32, no. 5, p. 677–684, 2005.

[11] K. Mukai, "Wetting and Marangoni effect in iron and steelmaking processes." *ISIJ International*, vol. 32, no. 1, p. 1–9, 1992.

[12] L. Zheng and X. Zhang, "Embedding-parameters perturbation method," *Modeling and Analysis of Modern Fluid Problems*, p. 39–77, 2017.

[13] E. Yildirim, "Modeling and analysis of a microfluidic capillary valve," *Politeknik Dergisi*, vol. 20, no. 2, pp. 487–494, 2017.

[14] C. Bouchenna, M. Ait Saada, S. Chikh, and L. Tadrist, "Investigation of thermocapillary flow inside an evaporating pinned water droplet," *Interfacial Phenomena and Heat Transfer*, vol. 3, no. 2, p. 185–201, 2015.

[15] E. Bormashenko, *Wetting Transitions*. Dordrecht: Springer Netherlands, 2012, pp. 2830–2837.

[16] Y. Han, Y. Liu, M. Kaneko, and F. Uchikoba, "Wetting transition on heated microstructrured superhydrophobic surface," *AIP Advances*, vol. 9, no. 9, p. 095059, 2019.

[17] T. A. Sonia and C. P. Sharma, "Experimental techniques involved in the development of oral insulin carriers," *Oral Delivery of Insulin*, p. 169–217, 2014.

[18] S. Ok, J. Sheets, S. Welch, T. Liu, S. Kaya, and D. R. Cole, "Wetting behaviors of fluoroterpolymer fiber films," *e-Polymers*, vol. 20, no. 1, p. 393–410, 2020.

[19] S. Banerjee, "Simple derivation of Young, Wenzel and Cassie-Baxter equations and its interpretations," *arXiv: Materials Science*, 2008.

[20] M. Khosravi, B. Rostami, M. Emadi, and E. Roayaei, "Marangoni flow: An unknown mechanism for oil recovery during near-miscible CO_2 injection," *Journal of Petroleum Science and Engineering*, vol. 125, p. 263–268, 2015.

[21] J. Speight, "Analysis of oil from tight formations," *Shale Oil and Gas Production Processes*, p. 519–571, 2020.

[22] R. K. Zeytounian, *Convection in fluids: a rational analysis and asymptotic modelling*. Springer Science & Business Media, 2009, vol. 90.

[23] Y. Imai, T. Yamamoto, A. Sekimoto, Y. Okano, R. Sato, and Y. Shigeta, "Numerical investigation of the nano-scale solutal Marangoni convections," *Journal of the Taiwan Institute of Chemical Engineers*, vol. 98, p. 20–26, 2019.

[24] A. Karbalaei, R. Kumar, and H. Cho, "Thermocapillarity in microfluidics—a review," *Micromachines*, vol. 7, no. 1, p. 13, 2016.

[25] H. J. Lee, F. D. J, R. M. Corn, and H. H. Girault, "Marangoni flow in microchannels," *Electrochemistry Communications*, vol. 1, no. 5, p. 190–193, 1999.

[26] M. A. Hossain, M. Hafiz, and D. Rees, "Buoyancy and thermocapillary driven convection flow of an electrically conducting fluid in an enclosure with heat generation," *International Journal of Thermal Sciences*, vol. 44, no. 7, p. 676–684, 2005.

[27] J. Chen, J. Wang, Z. Deng, X. Liu, and Y. Chen, "Experimental study on Rayleigh-Bénard-Marangoni convection characteristics in a droplet during mass transfer," *International Journal of Heat and Mass Transfer*, vol. 172, p. 121214, 2021.

[28] B. Arendt and R. Eggers, "Interaction of Marangoni convection with mass transfer effects at droplets," *International Journal of Heat and Mass Transfer*, vol. 50, no. 13-14, p. 2805–2815, 2007.

[29] J. Park, J. Ryu, H. J. Sung, and H. Kim, "Control of solutal Marangoni-driven vortical flows and enhancement of mixing efficiency," *Journal of Colloid and Interface Science*, vol. 561, p. 408–415, 2020.

[30] T. Yano, K. Nishino, S. Matsumoto, I. Ueno, A. Komiya, Y. Kamotani, and N. Imaishi, "Report on microgravity experiments of dynamic surface deformation effects on Marangoni instability in high-Prandtl-number liquid bridges," *Microgravity Science and Technology*, vol. 30, no. 5, p. 599–610, 2018.

[31] K. Nishino, T. Yano, H. Kawamura, S. Matsumoto, I. Ueno, and M. K. Ermakov, "Instability of thermocapillary convection in long liquid bridges of high Prandtl number fluids in microgravity," *Journal of Crystal Growth*, vol. 420, p. 57–63, 2015.

[32] A. Cihat Baytas and K. Cicek, "A numerical study of combined natural and Marangoni convection in a square cavity," *Marine Navigation and Safety of Sea Transportation*, 2009.

[33] N. Biswas and N. K. Manna, "Magneto-hydrodynamic Marangoni flow in bottom-heated lid-driven cavity," *Journal of Molecular Liquids*, vol. 251, p. 249–266, 2018.

[34] Z. Zheng, L. Zhou, X. Du, Y. Yang, P. Jiang, and B. Wang, "Numerical investigation on Marangoni convection of binary fluids in a closed microcavity," *Applied Thermal Engineering*, vol. 88, p. 464–472, 2015.

[35] G. J. Amador, Z. Ren, A. F. Tabak, Y. Alapan, O. Yasa, and M. Sitti, "Temperature gradients drive bulk flow within microchannel lined by fluid–fluid interfaces," *Small*, vol. 15, no. 21, p. 1900472, 2019.

[36] T.-m. Cai, Z.-h. Jia, H.-n. Yang, and G. Wang, "Investigation of Cassie-Wenzel wetting transitions on microstructured surfaces," *Colloid and Polymer Science*, vol. 294, no. 5, p. 833–840, 2016.

[37] T. Baier, C. Steffes, and S. Hardt, "Thermocapillary flow on superhydrophobic surfaces," *Physical Review E*, vol. 82, no. 3, 2010.

[38] H. Hanaei, M. K. Assadi, and R. Saidur, "Highly efficient antireflective and self-cleaning coatings that incorporate carbon nanotubes (CNTS) into solar cells: A review," *Renewable and Sustainable Energy Reviews*, vol. 59, p. 620–635, 2016.

[39] T. Darmanin and F. Guittard, "Superhydrophobic and superoleophobic properties in nature," *Materials Today*, vol. 18, no. 5, p. 273–285, 2015.

[40] A. Mall, P. Jelia, A. Agrawal, R. Singh, and S. Joshi, "Design of arrayed micro-structures to get super-hydrophobic ... - comsol," 2009. [Online]. Available: https://comsol.com/paper/download/46251/Joshi.pdf

[41] B. Gale, M. Eddings, S. Sundberg, A. Hatch, J. Kim, T. Ho, and S. Karazi, "Low-cost MEMS technologies," *Reference Module in Materials Science and Materials Engineering*, 2016.

[42] S. Tayyaba, M. W. Ashraf, Z. Ahmad, N. Wang, M. J. Afzal, and N. Afzulpurkar, "Fabrication and analysis of polydimethylsiloxane (PDMS) microchannels for biomedical application," *Processes*, vol. 9, no. 1, p. 57, 2020.

[43] T. N. Le, V.-A. Nguyen, G. L. Bach, L. D. Tran, and H. H. Cao, "Design and fabrication of a PDMS-based manual micro-valve system for microfluidic applications," *Advances in Polymer Technology*, vol. 2020, p. 1–7, 2020.

[44] S. Banik, A. Uchil, T. Kalsang, S. Chakrabarty, M. A. Ali, P. Srisungsitthisunti, K. K. Mahato, S. Surdo, and N. Mazumder, "The revolution of PDMS microfluidics in cellular biology," *Critical Reviews in Biotechnology*, p. 1–19, 2022.

[45] R. H. Farahi, A. Passian, T. L. Ferrell, and T. Thundat, "Microfluidic ma-

nipulation via Marangoni forces," *Applied Physics Letters*, vol. 85, no. 18, p. 4237–4239, 2004.

[46] J. Berthier, "The physics of droplets," *Micro-Drops and Digital Microfluidics*, p. 75–160, 2013.

[47] C. Y. A. and J. M. Cimbala, *Fluid Mechanics: Fundamentals and Applications*. McGraw-Hill Education, 2018.

[48] B. E. Rapp, *Microfluidics: Modeling, mechanics and mathematics*. Elsevier, 2022.

[49] "Understanding, and changing, the element order." [Online]. Available: https://www.comsol.com/support/knowledgebase/1270

[50] J. E. Mark. Oxford University Press, 2009, p. 411–435.

[51] R. K. Annavarapu, S. Kim, M. Wang, A. J. Hart, and H. Sojoudi, "Explaining evaporation-triggered wetting transition using local force balance model and contact line-fraction," *Scientific Reports*, vol. 9, no. 1, 2019.